Sustainable Cities and Society 47 (2019) 101419

Contents lists available at ScienceDirect

Sustainable Cities and Society

journal homepage: www.elsevier.com/locate/scs

Analysis of spatial and temporal distribution patterns of temperatures in urban and rural areas: Making urban environmental climate maps for supporting urban environmental planning and management in Hiroshima

Kaoru Matsuo[a,*], Takahiro Tanaka[b]

[a] Graduate School of Engineering, The University of Tokyo, 7-3-1 Hongo, Bunkyo-ku, Tokyo 113-8656 Japan
[b] Graduate School of Engineering, Hiroshima University, 1-4-1 Kagamiyama, Higashi-Hiroshima, Hiroshima 739-8527, Japan

ARTICLE INFO

Keywords:
Urban Environmental Climate Maps (UECMs)
Urban Heat Island
WRF
Field Measurement
GIS

ABSTRACT

Urban planning incorporating mitigation of the urban warming which is due to urban heat island phenomena and climate change is needed. However, such planning is not realized. That is apparently because the urban climate phenomenon is difficult to understand for stakeholders: citizens, planners, architects, specialists, and so on. Urban Environmental Climate Maps (UECMs) are therefore proposed as one of the decision support tools for the urban warming mitigation. Accordingly, the authors intend to produce UECMs in Hiroshima as the final goal of this study. Therefore, for the production of UECMs, this study aims to analyze the relationship between spatial temperature distribution and the comprehensive factors using observed data and numerical simulation results and perform climate zoning based on these results in Hiroshima. This study progressed via the following steps: 1) classifying Hiroshima area into the plain area and the mountain area; 2) analysis on the causes of temperature distribution based on observed data in the plain area; 3) analysis on the effect of sea breeze on summer diurnal temperature distribution patterns; 4) analysis on the causes of temperature distributions based on observed data in the mountain area; and 5) urban climate zoning and construction of UECMs.

1. Introduction

1.1. Background

Urban warming, which is due to urban heat island phenomena and climate change, has negative effects on the comfort of the outdoor environment, the health of inhabitants, the energy consumption for cooling and the urban ecosystem. It is hoped that the mitigation of urban warming will improve (Architectural Institute of Japan, 2007). In Japanese local governments and relevant ministries, planning and guidelines for this mitigation have been established such as the Osaka Heat Island Measures Promotion Plan in Osaka prefecture and Osaka city (2015) or the "countermeasures guideline for urban heat island" in Sakai city (2008). The Policy Framework to Reduce Urban Heat Island Effects was also established by the Inter-Ministry Coordination Committee to Mitigate Urban Heat Island (2004). It indicated five pillars of countermeasures to urban heat islands: 1) reduction of anthropogenic heat emissions, 2) improvement of urban surfaces, 3) improvement of urban structures, 4) improvement of lifestyles, and 5) promotion of adaptation. Recently, The Ministry of Land, Infrastructure, Transport and Tourism (2015) considered a countermeasures plan for urban heat island in the Climate Change Adaptation Plans. In such context, urban warming has become a subject of social concern.

However, there are few examples of planners (or stakeholders) considering urban warming mitigation based on scientific knowledge in their planning processes. This is apparently because the urban climate phenomenon is difficult to understand for stakeholders such as residents, local government officials, designers, and planners. The *Klimaatlas* (a German climate atlas) is therefore proposed as a tool for supporting urban planning (Architectural Institute of Japan, 2000). The role of these maps is to provide information from an urban climate perspective to decision-makers (including the public). In the Klimaatlas, the essence of climate research results by experts is described. When stakeholders (citizens, planners, architects, specialists, and others) make decisions about urban planning, architectural design, and environmental policies, they can use these maps as communication tools, like those used by other experts such as climatologists. Therefore, the purpose of creating these maps is to support the making urban planning or design proposals by stakeholders to mitigate urban warming.

* Corresponding author.
E-mail address: cafeaulait.2125@gmail.com (K. Matsuo).

https://doi.org/10.1016/j.scs.2019.01.004
Received 20 April 2018; Received in revised form 19 September 2018; Accepted 2 January 2019
Available online 18 February 2019
2210-6707/ © 2019 Elsevier Ltd. All rights reserved.

1.2. The Klimaatlas

In German, “klima” means climate and “atlas” means maps. In a broad sense, Klimaatlas is defined as “maps that are intended to understand the regional climatic environment well” (Architectural Institute of Japan, 2000). In German cities, Klimaatlas is subject to utilization by urban planners in a narrow sense, in that they have been made or are utilized with the aim of planning for the mitigation of atmospheric pollution. However, in recent times, the Klimaatlas has been used in the adaptation to global warming. The production method of the Klimaatlas is standardized and their production guidelines are published by Verein Deutscher Ingenieure (1997).

The Klimaatlas for atmospheric pollution mitigation has been produced based on these guidelines in various regions in Germany. For example, in Stuttgart, climate analysis maps are made by overlaying the survey results of land use in a region with atmospheric pollution distribution, wind distribution, and temperature distribution (Architectural Institute of Japan, 2000). By using these maps, the “klimatope (minimum climate zones that are regarded as having the same climatic characteristic in cities or regions),” wind flow, source location of air pollution, and area of influence in targeted areas can be identified. The climatic recommendation map for urban planning and design is also based on this climate analysis map (Architectural Institute of Japan, 2000) and shows two area types: “natural areas” that should be preserved and “city areas” that should be improved, according to the degree necessary in a targeted area. Such maps are made for many cities, including Essen (Verein Deutscher Ingenieure, 2015). Also, in Kommunalverband Ruhr, the hint map (showing recommendations and climatic resources) for each municipality is made using a climatic analysis map for the municipalities’ union. The hint map in Kommunalverband Ruhr shows the area divided by building density and countermeasures for mitigating air pollution that should be performed in those areas (Verein Deutscher Ingenieure, 1997).

As these Klimaatlas concepts spread from Germany to other European cities, various Klimaatlases have been made in each region. In the 1980s and later, especially, these were made to include not only air pollution but also urban warming measurements (Ng & Ren, 2015). Such maps are called Urban Environment Climate Maps (UECMs). (Abbreviations used in this study are summarized in Table 1).

1.3. Klimaatlas cases for urban warming measurements (UECMs)

Around 2000, *Klimaatlas of Urban Environment: Urban planning with using the climate information* was published, and UECMs for urban warming measurements or similar maps have since been produced in Japan (Architectural Institute of Japan, 2000). Such maps, which show the condition of ground surfaces and wind, are made by overlaying arrows indicating prevailing wind directions or wind rose based on observational data on the land use map/land cover map or topographic map. This type of map is defined as Type A (Fig. 1). For example, a map showing hourly wind direction and wind speed in a target area by using the arrows on the “klimatope” was made for Kobe City (Moriyama & Takebayashi, 1998). The “klimatope map” was made based on the Normalized Vegetation Index (NVI) constructed from satellite data (LANDSAT-TM), because these zones are decided according to heat balance near the ground surface (Moriyama & Takebayashi, 1999). As with this case, a map was produced by overlaying the wind rose according to observational data and arrows indicating the prevailing winds (e.g., sea breezes) on the land use map of Osaka City (Tanaka & Moriyama, 2004). In Sendai City, as well, the map was made in the same way on a land cover map produced by satellite images (Watanabe & Junimura, 2004). In Tokyo, the map was made by overlaying arrows indicating wind paths and using numerical simulation results on a land use map (Ojima, 2010). These maps (Type A) are considered useful for stakeholders in urban planning such as local governments, citizens, planning consultants, and architects, who are attempting to understand the present climate conditions in a target area. However, it is difficult to examine suitable measurements that are advanced from that understanding using Type A maps.

Table 1
The abbreviations list of this study.

Abbreviations	Description
UECMs	Urban Environmental Climate Maps
GIS	Geographic Information System
UCMS	Urban Climate Map System
LCZ	Local Climate Zone
WRF	Weather Research & Forecasting
PC scores	Principal Component Scores
PCA	Principal Component Analysis
AVSE	Average Value of Surrounding Elevation
DCDS	Distance from the Coastline in the Direction of Sea Breeze
RBB	Rate of Building Blocking
NDVI	Normalized Difference Vegetation Index
RA	Surrounding River Area
UCM	Urban Canopy Model
TPI	Topographic Position Index
AI	Amount of Insolation
ACA	Amount of Cold Air
N	North
NNE	North-northeast
NE	Northeast
ENE	East-northeast
E	East
SE	Southeast
SSE	South-southeast
S	South
SSW	South-southwest
SW	Southwest
WSW	West-southwest
W	West
NW	Northwest
NNW	North-northwest

Therefore, another type of map was produced, showing the characteristics and subjects in each zone of a targeted area and classifying them according to surface conditions related to the local climate. This type of map is defined as Type B (Fig. 1). For example, in Tokyo, Japan, the “Thermal Environmental Map” was produced (Bureau of the Environment, Tokyo Metropolitan Government, 2005). This map showed some problem zones, classified by atmospheric heat load characteristics from surfaces or buildings in the 500 m mesh and then extracted. Specifically, the targeted area was classified by the results of a multivariate analysis (principal component analysis and cluster analysis) performed by using anthropogenic heat or land cover data. Maps in Osaka (Itada, 2006) and Yokohama (Samata, Inoue, Fukuda, & Hirasawa, 2006) cities were made using the same method. The map made by the Ministry of the Environment also corresponds to Type B. Actually, Problem areas where the quantity of sensible convective heat, anthropogenic heat (sensible heat), and building coverage rate are extensive are shown on this map using the results of Geographic Information System (GIS) analysis. Moreover, the above “klimatope map” broadly belongs to Type B.

There are many examples of Type B maps in the world. In Hong Kong, Ng and Ren (2015) made the “Urban Climatic Analysis Map” and “Urban Climatic Recommendation Map.” As for the actual method of production, the maps were first made by using the results related to the potential for urban warming (thermal load) and availability of wind (dynamic potential); these were evaluated by arithmetic calculations using GIS. The “Urban Climatic Analysis Map” was then made by overlaying the map of “Wind Information” on these two kinds of maps. Finally, the “Urban Climatic Recommendation Map” was made using the assessed values of the “Urban Climatic Analysis Map.” From this map, the problem areas of urban warming or weak winds, and the measurements for these problems can be understood. In Lisbon, Portugal, Alcoforado, Andrade, Lopes, and Vasconcelos, (2009) made

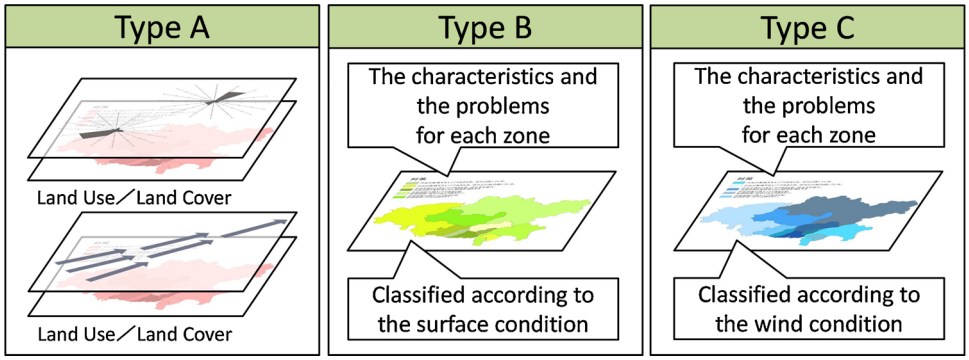
Type A
Land Use／Land Cover
Land Use／Land Cover
Type B
The characteristics and the problems for each zone
Classified according to the surface condition
Type C
The characteristics and the problems for each zone
Classified according to the wind condition

Fig. 1. The three types conceptual diagram of Urban Environmental Climate Maps (UECMs).

"Homogeneous Climate-Response Units." For their actual production, the targeted area was first classified as eight areas, using the results of arithmetic calculations performed on satellite image data and land cover data. Second, the climatic guideline for urban planning was shown in each classified area. Ren et al. (2012) suggested the production process of UECMs, "Urban Climate Map System (UCMS)," and the availability of UCMS is shown by producing the map in Arnhem as a case study. In Kaohsing, Taiwan, Ren, Lau, Yiu, and Ng, (2013) also made the "Urban Climatic Map" by overlaying observed data of wind direction on a map that the factors of temperature distribution such as land use data or water body data were summarized into the 500 m mesh. In this case, recommended examples of building arrangements or desirable areas where green areas and water spaces are positioned were shown according to each factor's temperature distribution. Acero, Arrizabalaga, Kupski, and Katzschner, (2013) made the "Urban Climate Analysis Map" and "Urban Climate Recommendation Map" using the arithmetic calculation results of GIS data, building volume, building surface fractions, green areas, ventilation paths, and slopes. From these maps, the climatic environment of the targeted area, especially the potential for ventilation, can be understood. He, Shen, Miao, Dou, and Zhang, (2015) produced the "Thermal Load Map" using the data of topographic height, sky view factor, open water, and green space, and the "Ventilation Potential Map" using data on building heights, roughness length, building coverage, and woodland areas. The "Urban Climatic Analysis Map" was made by overlaying these two maps. Recently, cases in which zoning is determined using the Local Climate Zone (LCZ) stand out (Cai, Ren, Xu, Dai, & Wang, 2016). LCZs are made through arithmetic calculations using GIS, in accordance with Oke's thinking on this matter (Stewart & Oke, 2012). It is thought that many klimaatlas is produced internationally because the above cases are similar to Type B.

As for Type B, the area is classified according to surface condition alone by using a mesh and so on. However, temperature distribution is formed not only by surface conditions but also by regional wind conditions, for example, sea and land breezes. It is necessary to classify the zones by regional wind condition. Such maps have been made recently, and in this study, this kind of map is defined as Type C (Fig. 1). Tanaka and Moriyama (2011) made a Type C map, for example, after Type A map ("Urban Climatic Analysis Map") was made in Sakai, Osaka. In practice, the area was gradually classified as "the area where sea and land breezes blow" and "the area where sea and land breezes do not blow" by using the average wind speed that is calculated for each 1 km mesh during a specified period using the wind speed distribution results of the Fifth-Generation NCAR / Penn State Mesoscale Model (MM5). In Osaka, Kitao, Moriyama, Takebayashi, and Tanaka, (2012) also made a map that shows the expected degree of using wind. In particular, that map is classified by using the average wind speed for each 1 km mesh during a specified period which is calculated by the wind speed distribution results of the meso-scale numerical simulation model Weather Research & Forecasting (WRF) model. In the area where the expected degree of using wind is low, it is necessary to improve the land cover and carry out the relative measurements of solar shading.

UECMs of a complex type such as Type B and Type C are considered preferable because the temperature distribution in each location in an urban area is formed not only by surface conditions but also by regional wind conditions. Mouri, Oba, Mochida, Yoshino, and Watanabe, (2008) made a map showing the area where measurements for land cover or ventilation condition are required by using comparisons of the heat balance structure in each area based on simulation results in Sendai. Such maps have characteristics of the complex Type B and C maps because it has the influence of regional wind and surface heat balance added.

According to the above example, it is effective to use a mesoscale meteorological model to classify the zones by regional wind conditions, considering the mechanism of how it was formed. However, it is difficult to consider local influences such as the effects of surrounding buildings or surrounding green areas because the spatial resolution of numerical simulation is about 1 km in the case of numerical simulations of the urban scale. Therefore, an effective method is to make UECMs using the observed data influenced by the local climate and indicate the mechanisms causing such phenomena by using the numerical simulation as evidence. Also, it has been pointed out that simulation concerning the social or economic problems do not have high reliability in Japanese society (Terano, 2012). It is considered effective to explain urban climate phenomena mainly by the analysis of observed data and numerical simulation results as evidence because climate simulations are the same on such points.

With respect to the final content of the planning recommendations shown on the map, Tanaka and Moriyama (2011) shows that the urban climate recommendation map of the planning-support types, on which recommendations for planning or usable climatic resources for mitigation are shown for each zone, is effective. In other words, a map that contained the menu of recommendations for each zone is required to take zoning one step further. There are some maps at the district level as UECMs have satisfied such needs. Narumi, Mizuno, and Shimoda, (2002) made a map showing recommendations for planning (e.g., utilization of cold air drainage or solar energy) for each of six zones that were classified using the results of observations (temperature and wind) and moving observations (temperature), and the ground topographical surface conditions in the hilly area of Kawanishi, Hyogo. Tanaka, Yamashita, and Moriyama, (2007) also made a map showing the area where the improvement of ventilation is preferable or the measurements for decreasing the surface temperature are necessary given the surface conditions or the thermal images photographed from the sky in the coastal area in Nagata, Kobe. In this case, a planning workshop was conducted and a planning concept map was made by using that map. The district level is targeted in these two cases. However, the urban climate recommendation maps for planning support are also needed at the city level which is larger than the district level.

From the above background, it is apparent that UECMs should

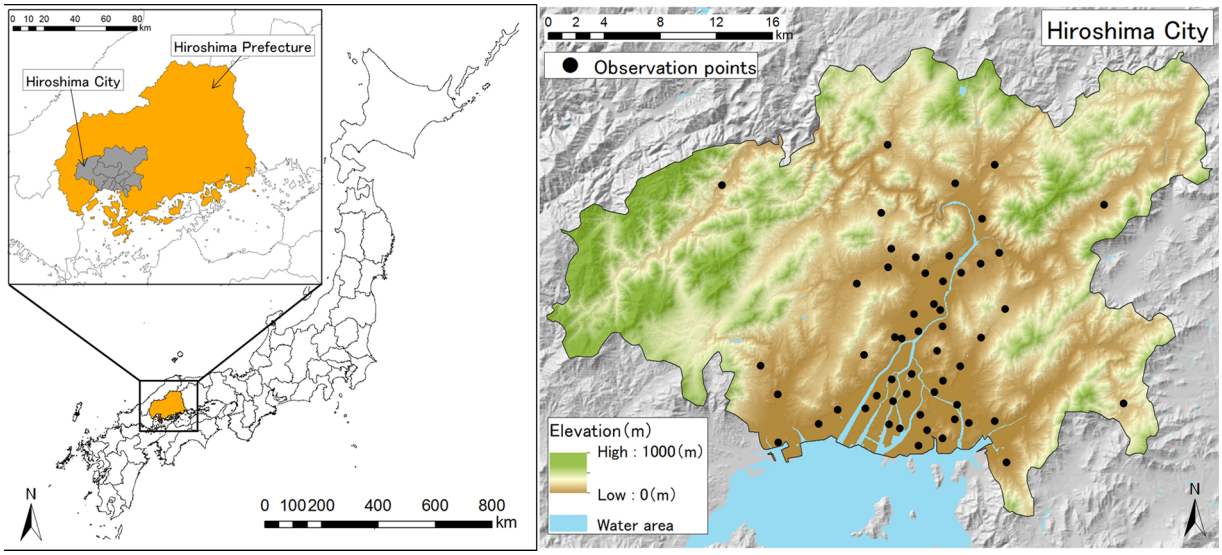

Fig. 2. The outline of targeted area and the location of observation points.

satisfy the following conditions in addition to conventional conditions.

1 UECMs should be made according to analyses of observed data. The mesoscale meteorological model is used to indicate the mechanisms causing climate phenomena.
2 UECMs should be of the complex type, such as Type B and C, because the urban climate is formed by surface conditions and wind conditions.
3 Recommendations for planning or usable climatic resources for mitigation must be shown in each zone. It is necessary to understand factors affecting temperature distribution patterns in each zone.

To produce UECMs that satisfy the above conditions, this study aims to analyze the relationship between spatial temperature distribution and comprehensive factors using observed data and numerical simulation results and perform climate zoning based on these results in Hiroshima.

1.4. Outline of study area

In this study, Hiroshima is selected as the targeted area (Fig. 2). In Hiroshima, a plain is formed around the Otagawa Delta. A hilly area spreads out to the surrounding plain. In addition, sea and land breeze circulation is observed in the southern area facing the sea. In this area especially, located between the Shikoku Mountains and Chugoku Mountains, there are often sea and land breezes because seasonal winds are infrequent (Miyata, 1982).

1.5. Method

This study undertook the following steps.

1) Area zoning based on climatic characteristics;
2) Analysis of the causes of temperature distribution based on observed data in the plains area;
3) Analysis of the effect of sea breezes on the summer diurnal temperature distribution pattern;
4) Analysis of the causes of temperature distribution based on observed data in the mountain area;
5) Urban climate zoning and production of UECMs

This study is also significant and original for the following points.

(1) Determining the three conditions on which UECMs should be made in the future by organizing previous studies about UECMs.
(2) Evaluating factors comprehensively by using meteorological observation temperature data of the plain and mountain area.
(3) Understanding the effect of sea breeze on summer diurnal temperature distribution patterns by using meteorological observation temperature data and numerical simulation results.
(4) Constructing UECMs based on the results of (2) and (3).

2. Area zoning based on climate characteristics

2.1. Outline of meteorological observations

Initially, 64 temperature sensors in instrument screens were set in Hiroshima. Basic information related to the observation points is given below.

- Period: from July 20, 2013 to September 23, 2013
- Observation interval: 10 minutes
- Instrumental error: corrected

The results of 60 observation points were used in this analysis because four observation points were missing (Fig. 2). The observation results were calibrated using an incubator.

2.2. Extracting fine-weather days

Initially, fine-weather days (35 days) were extracted from all data (66 days) in the observation period by applying the local meteorological station according to the criteria (Table 2).

2.3. Wind pattern classification of fine-weather days

From the above classification, the data from 35 fine-weather days were used. The wind blowing pattern classification was made using

Table 2
The criteria of extracting fine-weather days.

- Daily precipitation is within 1 mm.
- Daylight hours (i.e., the time observed by the sunshine recorder) constitute 40% or more of the possible duration of sunshine (i.e., the time from sunrise to sunset).
- Daily maximum temperature is more than 30 °C.
- The weather is not rainy.

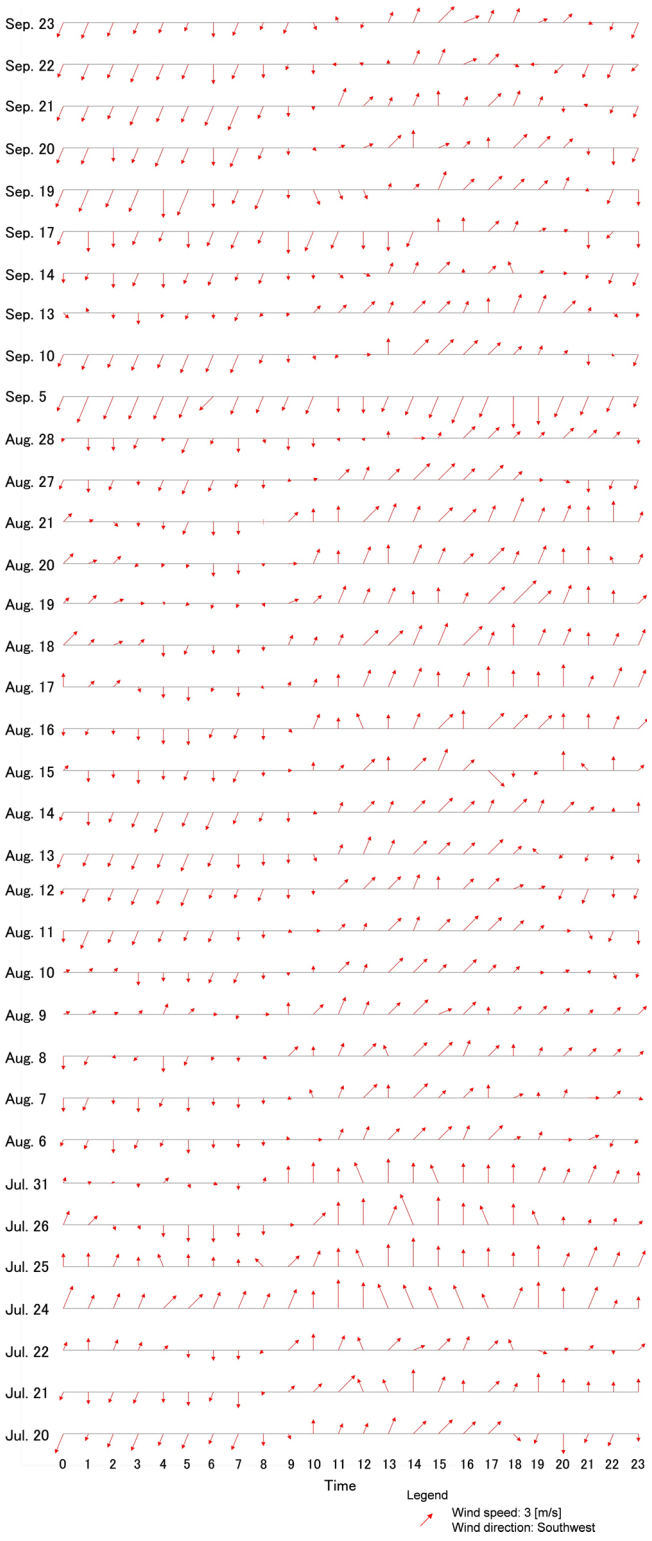

Fig. 3. Wind speed and wind direction of fine-weather days (35 days).

only the wind direction and speed data from the local meteorological station. Some measurement data (wind speed and wind direction) are shown in Fig. 3 and winds rose are shown in Fig. 4. It is apparent that several different types of daily wind-direction change patterns exist. In these patterns, it can be seen that the proportion of days when land and sea breezes blow (from the south in the daytime and from the north at nighttime) is high, but there are some days when wind blows from the north all day (e.g., Sep. 5) or from the south all day (e.g., Jul. 31).

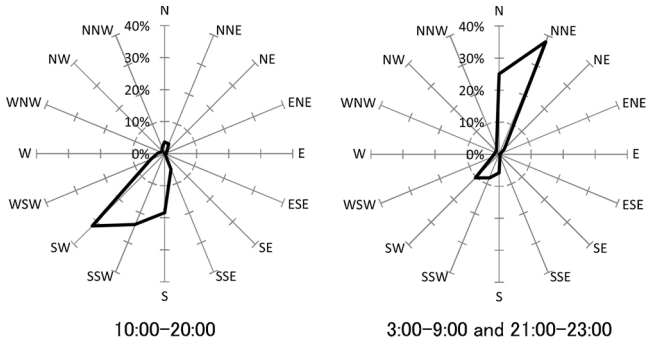

Fig. 4. The wind rose of fine-weather days (35days).

Therefore, classification criteria (Table 3) were defined on the basis of method proposed in a previous study (Miyata, 1982). Wind blowing pattern classification was performed by applying the wind-direction data (the local meteorological station, every hour on the hour) of fine-weather days (35 days) to these classification criteria. In this classification, “sea breeze” is defined as “wind blowing from the directions, SE, SSE, S, SSW, SW, WSW, and W” because the major sea breeze direction is SSW. Additionally, “land breeze” is defined as “wind blowing from the directions, NW, NNW, N, NNE, NE, ENE, and E.” These do not include wind from the ESE or WNW. As a result of the classification, the 35 fine-weather days can be classified into three patterns: Pattern A (sea breeze does not blow); Pattern B (sea breeze blows, but land breeze does not blow); and Pattern C (land and sea breezes blow) (Table 3). This table proves that the majority are Pattern C fine-weather days. Therefore, typical fine-weather summer days (29 days) are defined as Pattern C. The same classification was also performed from 2009 to 2012. This result proves that the wind conditions in the summer of 2013 were standard for the five-year period.

2.4. The temperature distribution of typical fine-weather summer days

The average daily maximum temperature and average daily minimum temperature of Pattern C are shown in Fig. 5. According to these figures, the temperature in coastal areas in daytime is relatively low, but the temperature in inland areas at night is also low. Given these results, it is assumed that temperature distribution patterns and their contributing factors are difficult to determine between the plains and the mountain areas. Therefore, a classification of observation points is performed for typical fine-weather summer days (29 days) for the area zoning based on climatic characteristics.

2.5. Classifying all observation points based on daily temperature change patterns

The classification of all observation points based on the daily temperature change patterns was performed in two steps. In step 1, principal component analysis was carried out. In step 2, cluster analysis was conducted using principal component scores (PC scores).

Principal component analysis (PCA) was conducted using six variables showing patterns of daily temperature change by using previous studies as a reference (Nabeshima, Nishioka, & Nakao, 2008). Table 4 presents the variables. Table 5 presents the PCA results. The first PC is apparently the “night temperature characteristic” because the PC loadings of “average temperature,” “minimum temperature,” “daily range,” and “degree-hour in the night” are high. The second PC is apparently the “daytime temperature characteristic” because the PC loadings of “maximum temperature” and “degree-hour in the daytime” are high scores.

In step 2, cluster analysis was performed using PC scores with Ward’s method. All observation points were classified into two clusters. Fig. 6 shows the results of this classification of observation points on the

Table 3
The wind blowing pattern classification criteria and results.

Wind pattern	Criteria	Classification result
Pattern A Sea breeze doesn't blow	1) Wind from the coast doesn't blow from 13:00 to 16:00 for more than 3 hours.	Sep. 5, Sep. 17
Pattern B Sea breeze blows, but land breeze doesn't blow	1) Wind from the coast blows from 13:00 to 16:00 for more than 3 hours. 2) Wind from the land doesn't blow from 3:00 to 6:00 for more than 3 hours.	July 24, July 25, July 31, Aug. 9
Pattern C Land and sea breeze blow (typical sea breeze day)	1) Wind from the coast blows from 13:00 to 16:00 for more than 3 hours. 2) Wind from the land blows from 3:00 to 6:00 for more than 3 hours.	July 20, July 21, July 22, July 26, Aug. 6, Aug. 7, Aug. 8, Aug. 10, Aug. 11, Aug. 12, Aug. 13, Aug.14, Aug. 15, Aug.16, Aug. 17, Aug. 18, Aug. 19, Aug. 20, Aug. 21, Aug. 27, Aug.28, Sep. 10, Sep. 13, Sep. 14, Sep.19, Sep. 20, Sep.21, Sep. 22, Sep. 23

- "sea breeze" is defined as "wind blowing from the direction, SE, SSE, S, SSW, SW, WSW, and W" because the major sea breeze direction is SSW.
- "land breeze" is defined as "wind blowing from the direction, NW, NNW, N, NNE, NE, ENE, and E" because the major land breeze direction is NNE.
- "sea breeze" and "land breeze" do not include wind from the ESE or WNW.

map. This figure shows that classification group 1 (C1) is in the plain area, while classification group 2 (C2) is in the mountain. There are also two types of climate characteristics in Hiroshima City mainly because of its geographical characteristics. Therefore, area zoning is proven according to the classification results of the observation points.

2.6. Area zoning based on the climate characteristic

From the results in the last section, it was assumed that climate characteristics differ between the plains and the mountain areas in Hiroshima. Therefore, area zoning was performed using the "average value of surrounding elevation (AVSE)." First, the average value and standard deviation of AVSE, which were calculated from 0 to 8000 m around temperature observations every 100 m, were calculated by clusters (AVSE_C1 and AVSE_C2). In these calculation results, there were significant differences between the average values of AVSE_C1 and AVSE_C2. Therefore, all differences (D_{AVSE}) were calculated using the expressions (1), (2), (3) and that difference was the maximum of those in the AVSE around 1100 m. The results were that the Hiroshima area was divided into two areas using the median value, M_e (79.2 m), of "the average value of AVSE_C1 around 1100 m" and "the average value of AVSE_C2 around 1100 m" as a threshold using the expression (4). The area below this threshold value (79.2 m) is defined as the plains area, while the area above it is defined as the mountain area.

$$\overline{AVSE_{C1}} = \frac{1}{N_{C1}}\sum_{i=1}^{N_{C1}} AVSE_{C1i} \quad \overline{AVSE_{C2}} = \frac{1}{N_{C2}}\sum_{i=1}^{N_{C2}} AVSE_{C2i} \tag{1}$$

$$s_{C1} = \sqrt{\frac{1}{N_{C1}}\sum_{i=1}^{N_{C1}} (AVSE_{C1i} - \overline{AVSE_{C1}})} \quad s_{C2} = \sqrt{\frac{1}{N_{C2}}\sum_{i=1}^{N_{C2}} (AVSE_{C2i} - \overline{AVSE_{C2}})} \tag{2}$$

$$D_{AVSE} = (\overline{AVSE_{C2}} - s_{C2}) - (\overline{AVSE_{C1}} + s_{C1}) \tag{3}$$

Table 4
The six variables showing patterns of daily temperature change.

Variables
1) Average temperature (degree C.)
2) Average of daily maximum temperatures (degree C.)
3) Average of daily minimum temperatures (degree C.)
4) Average daily range of temperatures (degree C.)
5) Integration of degree-hour in the daytime (degree C.*h)
6) Integration of degree-hour in the nighttime (degree C.*h)

Table 5
The PCA results.

Principal component	1st PC	2nd PC
Average temperature	***0.77***	0.63
Maximum temperature	−0.42	***0.90***
Minimum temperature	***0.97***	0.20
Daily range	***−0.92***	0.39
Degree-hour in the daytime	−0.23	***0.96***
Degree-hourin the nighttime	***0.95***	0.29
Eigenvalue	3.51	2.40
Contribution ratio (%)	58.51	40.03
Cumulative contribution ratio(%)	58.51	98.54

$$M_e = \frac{\overline{AVSE_{C2\_1100}} - \overline{AVSE_{C1\_1100}}}{2} \tag{4}$$

($\overline{AVSE_{C1}}$: The average values of AVSE_C1; $\overline{AVSE_{C2}}$: The average values of AVSE_C2; N: Sample size; $AVSE_{C1}$: AVSE_C1; $AVSE_{C2}$: AVSE_C2; s_{C1}: The standard deviation of AVSE_C1; s_{C2}: The standard deviation of AVSE_C2)

In Chapter 3 and 5, understanding the summer temperature

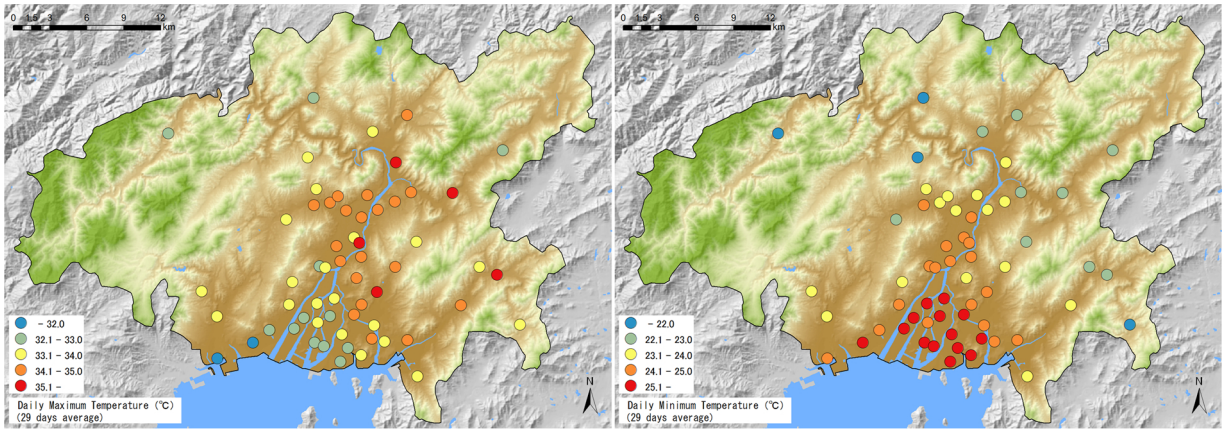

Fig. 5. The average daily maximum temperature and average daily minimum temperature of "pattern C.".

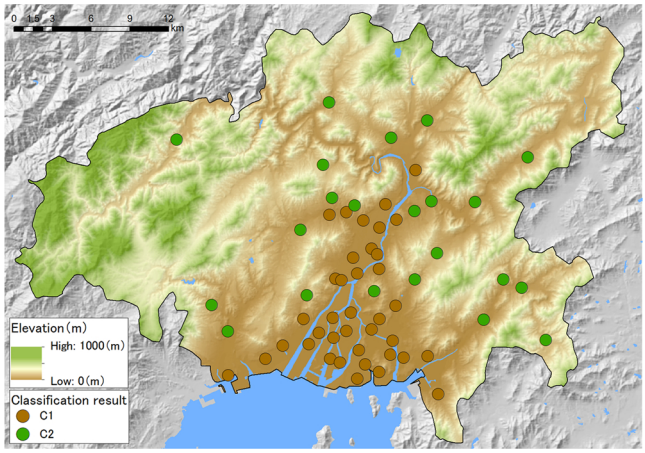

Fig. 6. The results of this classification of observation points.

distribution and comprehensively evaluating the contributory factors are conducted on these two areas (Fig. 7).

3. Comprehensively evaluating the factors of temperature distribution in the plains area

In Chapter 3, understanding the summer temperature distribution and evaluating its contributory factors comprehensively were undertaken using 39 observation points in the plains area (Fig. 7). For the temperature data, the typical fine-weather summer days (29 days), which were extracted in the preceding chapter, were targeted. Also, the temperature distribution factors, 1) distance from the coastline in the direction of the sea breeze, 2) local ventilation conditions, 3) surrounding green areas, and 4) the surrounding river area were targeted by using previous studies as references (Cai, Han, & Chen, 2018; Kiyota, Taniguchi, Kiyota, & Nakamura, 2007; Noguchi, Tanaka, & Sadohara, 2014; Ogawa et al., 2011). Factors 1), 2), and 3) were considered as those that had an effect on the temperature distribution in coastal cities. Factor 4) was considered to be the characteristic factor in delta areas.

3.1. Outline of temperature distribution factors

3.1.1. Distance from the coastline in the direction of the sea breeze

First, a numerical simulation was performed to understand the wind distribution in the entire plains area (the detailed outline of the numerical simulation is explained in Section 4.2.). The targeted period when the typical fine-weather summer days continued was from August

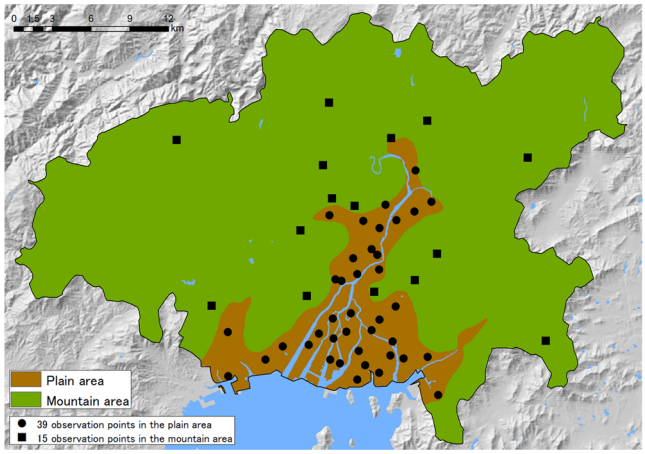
0 1.5 3 6 9 12 km
Plain area
Mountain area
39 observation points in the plain area
15 observation points in the mountain area

Fig. 7. The area zoning results using "the average value of surrounding elevation (AVSE)" and the located observation points in each area.

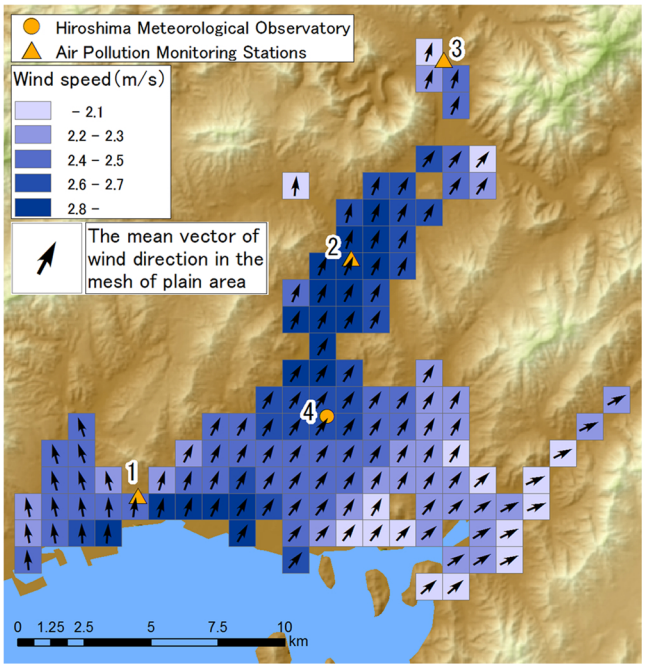

Fig. 8. The mean vector of wind speed and direction at 10 m in the plain area mesh based on the simulation results and the location of Hiroshima Meteorological Observatory and three air pollution Monitoring Stations.

4, 2013 to August 17, 2013. Fig. 8 shows the mean vector of wind speed and direction at 10 m in the plain area mesh. This was calculated using simulation results from 10:00 to 20:00 and from August 10 to August 16, apart from the spin-up time. Wind from the south-southwest was defined as prevailing in the plains area. On the other hand, the three air pollution monitoring stations showed that wind from the southwest prevailed, and the Hiroshima Meteorological Observatory showed that the wind from the south-southwest prevailed (Fig. 9). Giving comprehensive consideration to the simulation results and the observed data, the prevailing wind in the entire plains area was defined as south-southwest.

Next, a straight line was drawn in the south-southwest from each observed temperature point to the coastline. The distance of that line was defined as the "distance from the coastline in the direction of sea breeze (DCDS)."

3.1.2. Local ventilation conditions

The temperature is influenced not only by extended sea breeze (DCDS) but also by the ventilation conditions according to buildings around the observation points. Therefore, in this study, the index of the "rate of building blocking (RBB)" (Noguchi et al., 2014) was defined as these local ventilation conditions. The index shows the degree to which each observation point is blocked by surrounding buildings in three dimensions, which can also be calculated using GIS. The conceptual diagram of RBB is shown in Fig. 10, and the calculation method used is as follows.

1) First, the building data (polygon) are prepared to include the attribute of height and the observation point data (point). Next, the building data are raised by height attribute, while the observation point data are raised at 1.5 m.
2) The buffer polygon of radius r m of the observation point is calculated and raised at h m.
3) Initially, the line of sight from the observation point (skyline) is calculated using the three dimensional building data prepared in step 1). Next, the three dimensional area included in the buffer polygon (step 2)) under the skyline is calculated (skyline barrier).

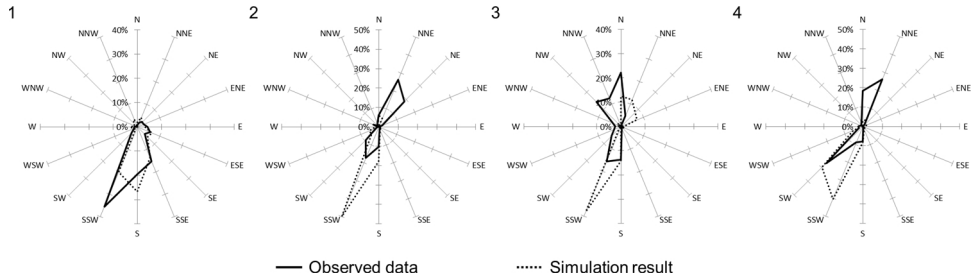

Fig. 9. The wind rose of Hiroshima Meteorological Observatory and three air pollution Monitoring Stations. The number (1,2,3,and 4) is related with Fig. 8.

4) The skyline barrier area is projected onto the ground (a projected area is made of the skyline barrier).
5) First, the specific direction part of the buffer polygon at the observation point (the quarter sector at the center of the specific direction) is extracted and a quarter sector polygon is made. Then, the projected area of the skyline barrier area is clipped by this quarter sector polygon.
6) RBB is calculated using the following expression (in the event that the specific direction is south-southwest). Also, the calculation method is the same in every direction.

$$A_{SSW} = \frac{(X - Y)}{X} \times 100 \quad (5)$$

(A_{SSW}: RBB%, X: The area of quarter sector polygon m^2, Y: The projected area of skyline barrier in the south-southwest m^2)

When the hourly correlation coefficient between RBB and the hourly average temperature of typical fine-weather summer days (29 days) have been calculated, the specific direction is defined in all directions and in four separate directions (north-northeast, east-southeast, south-southwest, west-northwest). Also, the combination of radius (r) and height (h) is defined in each direction for a total of nine patterns (radius: 50, 75, 100 m, height: 5, 10, 20 m). The results of every direction are shown in Fig. 11. From these figures, the correlation coefficient between "RBB in the direction of south-southwest and the combination of r = 100 m and h = 5 m" and the daytime temperature is high. On the other hand, at night, the correlation coefficient between "RBB in the direction of north-northeast and the combination of r = 100 m and h = 20 m" is also comparatively high. These results indicate that the temperature tends to be higher when RBB in the south-southwest is higher in daytime or RBB in the north-northeast is higher at night. This is because the sea breeze blows from the south-southwest in the day and the land breeze blows from the north-northeast at night. The reason the "height" of RBB shows the highest correlation with temperatures differing between day and night is the influence of "down blow" (a strong wind phenomenon occurring around a building. When a building is exposed to wind, the wind on the wall surface flows upward and downward separately, and the downward flow is called "down blow.") The down blow from buildings is small and the high buildings blocking it contribute to urban warming surrounding the observation points; this is because the wind speed and the extent of land breezes at night is minor, as pointed out in a previous study (Mori, Kitada, & Iyoda, 1998). Also, the correlation coefficient between temperature and RBB, which is calculated by the combination of r = 100 m and h = 5 m, is highest in cities in a basin (Noguchi et al., 2014). In daytime, the result is similar to the results of this study, but the result at night is different. One of the reasons for the difference is the influence of cold air drainage in cities that lie in a basin. However, in the next step, it is necessary to confirm the validation of the proper combination as the index of ventilation conditions at night.

Given the above consideration, the correlation coefficient between the temperature and RBB is the highest used in this study. In particular, the direction of south-southwest and the combination of r = 100 m and h = 5 m is defined as RBB in daytime (RBB-SSW) and the direction of north-northeast and the combination of r = 100 m and h = 20 m is defined as RBB at night (RBB-NNE).

3.1.3. Surrounding green area

The Normalized Difference Vegetation Index (NDVI), which is constructed from satellite data, (ASTER-VNIR) represents the surrounding green area (Fig. 12). NDVI is the vegetation index of the existence or non-existence of vegetation, and it shows the amount or activation level of the vegetation. Also, it has been proven that there is a correlation between NDVI and the green coverage ratio (Takeuchi, 1987).

In the previous study, the influence range of the surrounding average value of NDVI for temperature was within about 300 m radius (Irie & Hirano, 2001). Therefore, the surrounding average value of NDVI within 300 m (NDVI-300) is here defined as the index of the surrounding green area.

3.1.4. Surrounding river area

In this study, the river area ratio surrounding the observation point, which is calculated by using water area data, represents the surrounding river area. The conceptual diagram of the surrounding river

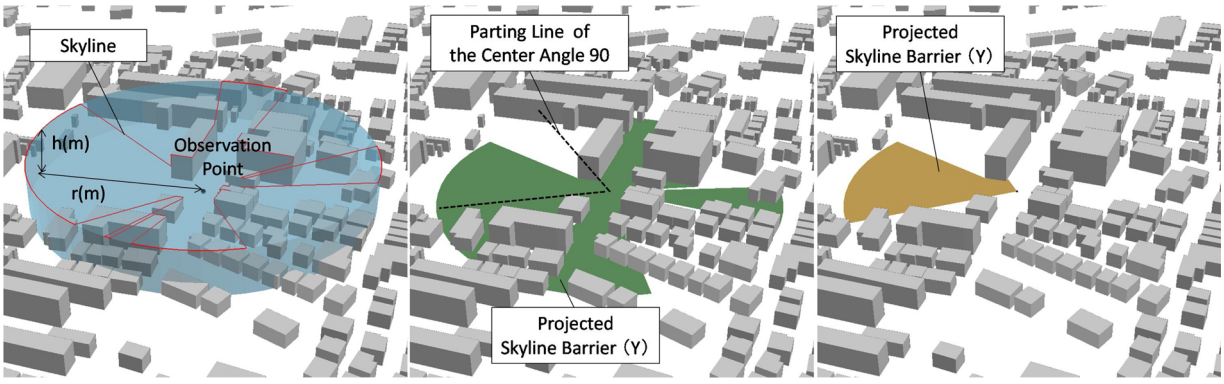

Fig. 10. The conceptual diagram of RBB.

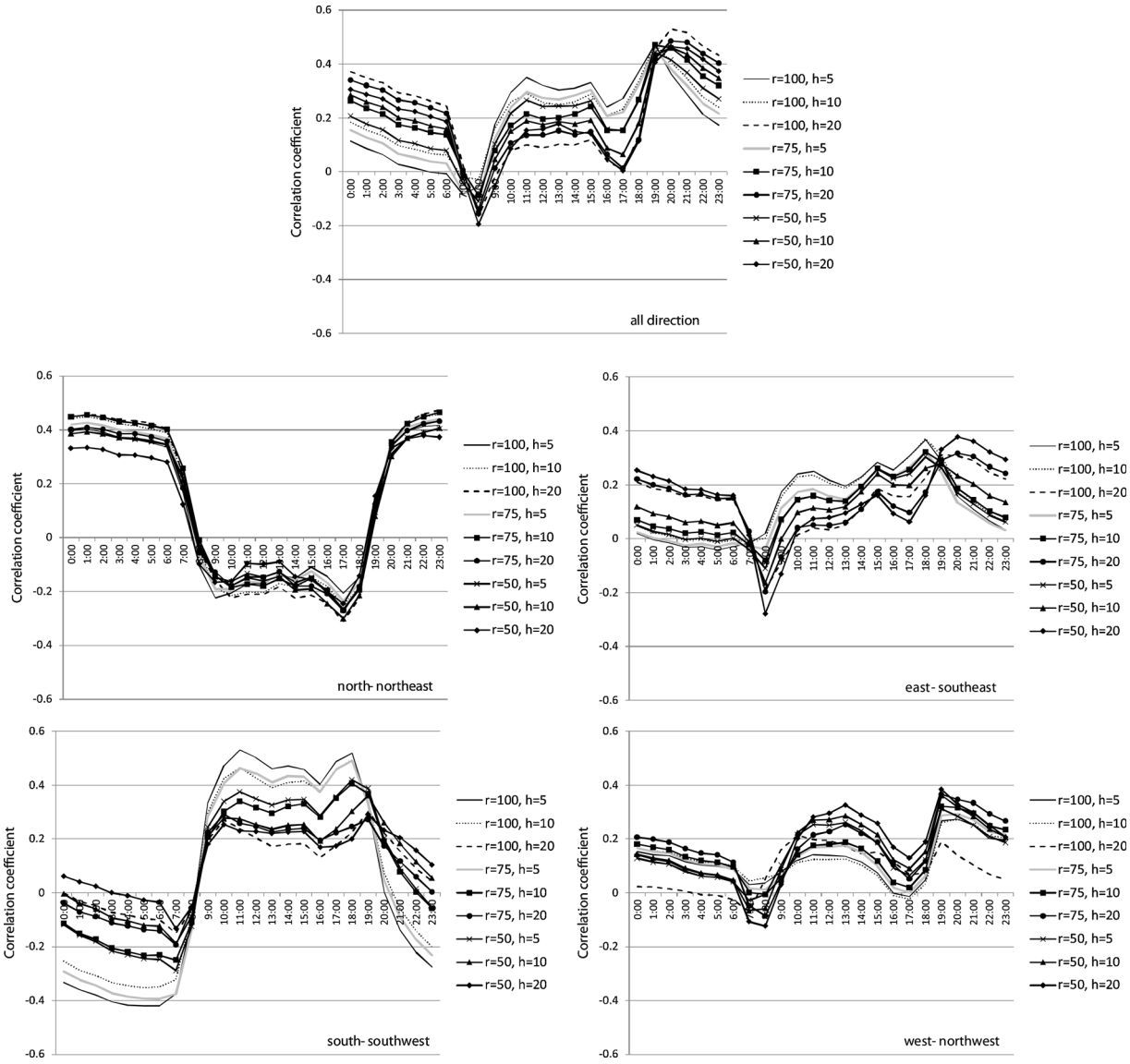

Fig. 11. The hourly correlation coefficient between RBB and the hourly average temperature of typical fine-weather summer days.

area is shown in Fig. 13. The surrounding river area within 300 m (RA-300) was defined as the index of surrounding river area because it is apparent from the previous study (Amano & Nakagawa, 2007) that the influence range of surrounding land cover characteristics for temperature were within a 300 m to 400 m radius; the surrounding green area was calculated within a 300 m radius in subsection 3.1.3..

3.2. Comprehensive evaluation using multiple regression analysis

In this section, multiple regression analysis was performed to comprehensively evaluate the influence of four factors on temperature. Specifically, multiple regression analysis was performed hourly using DCDS, RBB-SSW, RBB-NNE, NDVI-300, and RA-300 as explanatory variables, while the hourly average temperature of typical fine-weather summer days was treated as an objective variable. The correlation coefficient between explanatory variables is shown in Table 6. An hourly standard partial regression coefficient and multiple correlation coefficient are also shown in Fig. 14.

At first, the multiple correlation coefficient from 0:00 to 7:00 and from 12:00 to 18:00 is as high as 0.8; this multiple regression equation can explain objective variables with a determination coefficient of more than 0.6 in these time ranges. Next, the standard partial regression coefficient, DCDS, is high and RBB-SSW is slightly high in a positive direction in daytime. From these results, it was assumed that the summer temperature in the day had decreased from the influence of not only wind (sea breezes) in the direction of the south-southwest and but also surrounding ventilation conditions in windward. Also, it was confirmed that RBB-NNE is high in a positive direction, while NDVI-300 is high in a negative direction at night. From these results, it was assumed that temperatures at night decrease because of the influence of surrounding green areas and wind blowing in the north-northeast direction. In addition, the standard partial regression coefficient of DCDS was high in a negative direction, while the multiple correlation coefficient from 8:00 to 9:00 was relatively low. This is because factors other than those used in this analysis (such as sunlight) were related to the temperature during this period.

4. Analysis of the effect of sea breezes on summer diurnal temperature distribution patterns

The mechanism of temperature distribution is influenced by DCDS; the main factor was used in Chapter 3, and clarified by using the observed temperature in the plains area (39 points) and numerical simulation results.

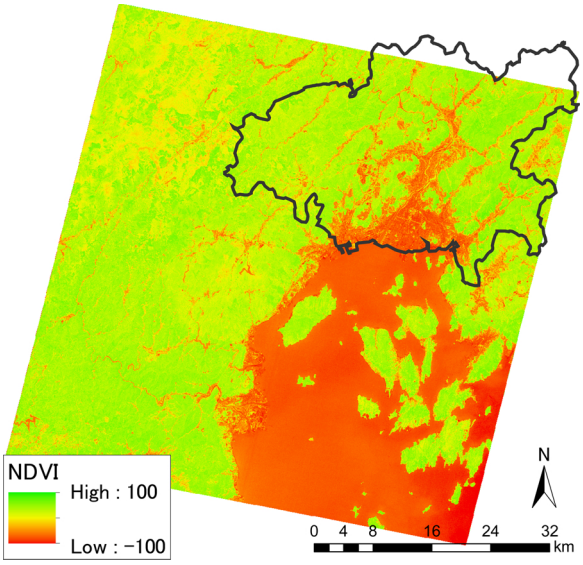

Fig. 12. The data of Normalized Difference Vegetation Index (NDVI) is constructed from satellite data, (ASTER-VNIR).

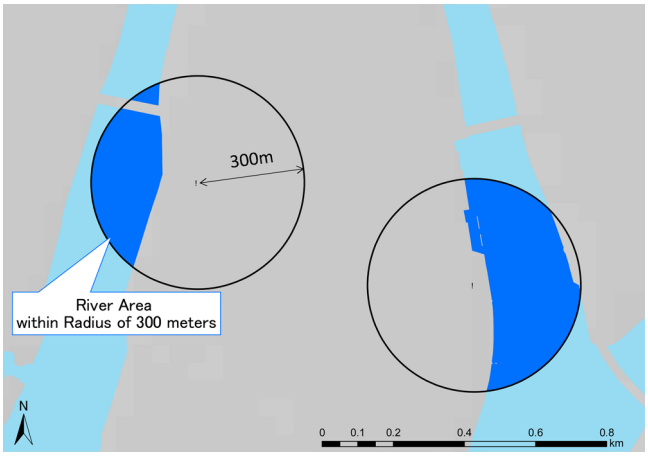

Fig. 13. The conceptual diagram of the surrounding river area.

Table 6
The correlation coefficients among the explanatory variables (plain area).

	DCDS	RBB-SSW	RBB-NNE	NDVI-300	RA-300
DCDS	1.00	0.46	−0.24	0.57	−0.22
RBB-SSW	−0.46	1.00	−0.11	0.43	−0.40
RBB-NNE	−0.24	−0.11	1.00	−0.20	−0.00
NDVI-300	0.57	0.43	−0.20	1.00	−0.32
RA-300	−0.22	−0.40	−0.00	−0.32	1.00

The mechanism is related to the influence of sea breezes. Therefore, at first, the sea breeze effect is defined as the temperature difference between Pattern A (sea breeze does not blow) and Pattern C (land and sea breezes blow) based on the previous study (Junimura & Watanabe, 2008). Next, the following three steps were undertaken to clear that mechanism.

1) Understanding the sea breeze effect distribution using the observed temperature of 39 points:

First, the sea breeze effect was defined as the temperature difference between Pattern A and Pattern C. The distribution of the sea breeze effect was then apparent.

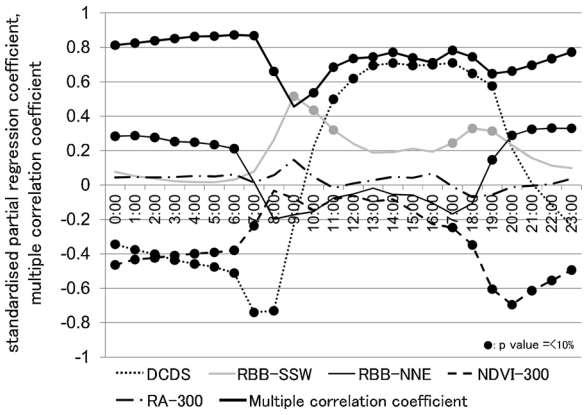

Fig. 14. The hourly standard partial regression coefficient and multiple correlation coefficient (Plain area).

2) Constructing the map of the sea breeze effect distribution using the mesoscale meteorological model:

First, the spatial distribution map of the sea breeze effect was produced using the result of the mesoscale meteorological model. Next, the validation of the sea breeze effect was confirmed by comparing it with the results of 1), and the sea breeze effect was quantitatively cleared by analyzing the sensible heat advection.

3) Analyzing the relationship between the observed temperature and the surrounding ventilation condition:

First, the target area was classified as the area where the sea breeze effect is large and the area where it is small based on the results of 2) (the spatial distribution map of sea breeze effect). Next, the influence on temperature mitigation in the local surrounding ventilation conditions produced by the difference of the sea breeze effect in regional areas was discussed by analyzing the relation between temperature and the surrounding ventilation condition (RBB) in those two areas.

4.1. Understanding sea breeze effect distribution using the observed temperature

4.1.1. Daily wind pattern classification

In this chapter, the observed temperature of Pattern C is targeted for analysis. First, examples of wind direction and speed on Pattern C are shown in Fig. 15. This figure shows two blowing patterns in Pattern C. The first pattern (C-1) shows the days on which the wind blows without a time lag between the coastal area and the inland area, while the second pattern (C-2) shows the days that the wind blows gradually from the coastal area to the inland area. Therefore, Pattern C is classified into these two blowing patterns by applying the criteria (Table 7) to the wind direction and speed data (air pollution monitoring stations). It was confirmed that 18 days were classified into C-1 and 11 days were classified into C-2.

4.1.2. Sea breeze effect distribution

The observed temperature difference between Pattern C-1 and Pattern A was first calculated using the method proposed in a previous study (Junimura & Watanabe, 2008). The observed temperature difference between Pattern C-2 and Pattern A was also calculated in the same way. This temperature difference was defined as the hourly sea breeze effect. In each pattern (C-1 and C-2), the sea breeze effect at 11:00 and 14:00 is shown in Fig. 16. From these figures, it can be seen that the sea breeze effect for mitigating urban warming is relatively larger in coastal areas and smaller in inland areas. Especially for the sea breeze effect at 11:00, there is no large difference in sea breeze effect

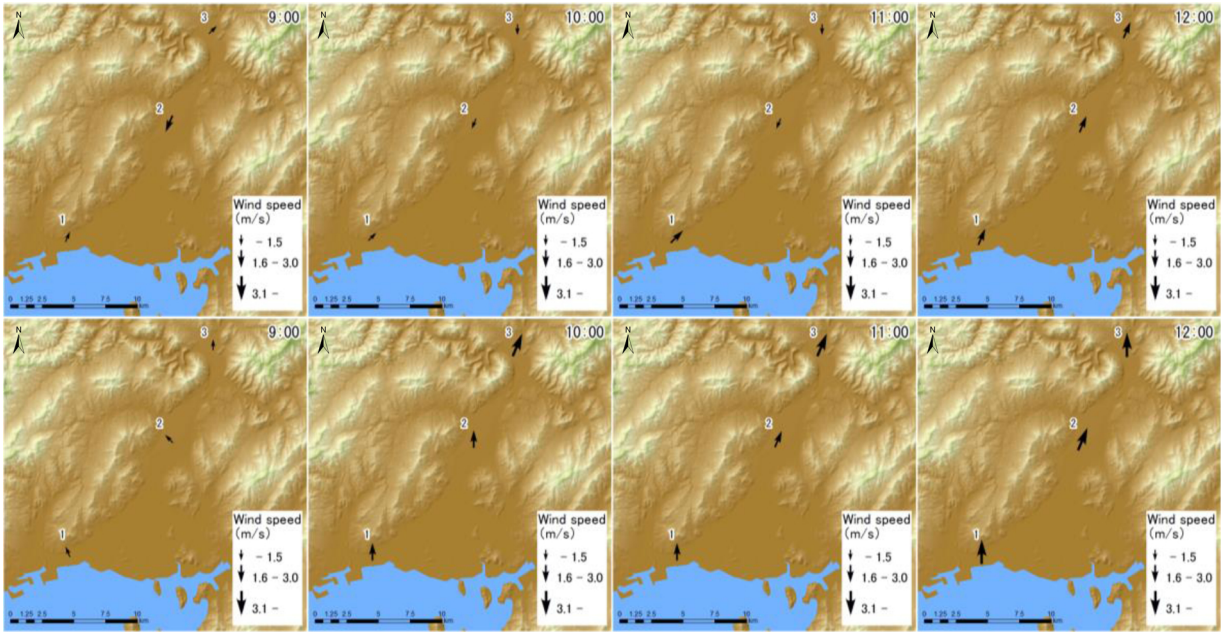

Fig. 15. The examples of wind direction and speed on pattern C.

distribution between Pattern C-1 and Pattern C-2, although there is a difference in the wind blowing patterns at 11:00. Therefore, for Pattern C-1, the effect of sea breezes for mitigating urban warming is small in inland areas at 11:00 and this wind seems to be different from the sea breeze.

Next, the hourly correlation coefficient of the sea breeze effect between Pattern C-1 and Pattern C-2 was calculated (Fig. 17). This figure indicates that these two patterns are similar. Therefore, the map of hourly sea breeze effect was constructed by using all of the data of Pattern C. The map at 14:00 is shown in Fig. 18 as an example.

4.2. Making the map of sea breeze effect distribution using the mesoscale meteorological model

4.2.1. Usage model and calculation condition

WRF-ARW ver. 3.0 (Skamarock et al., 2008) was used in this study. The calculation domain is shown in Fig. 19 and the calculation conditions are shown in Table 8. A nesting technique was used: Domain 1 is a 120 × 120 grid with a spatial resolution of 3 km. Domain 2 is a 103 × 103 grid with a spatial resolution of 1 km. The calculation periods were from August 4, 2013 to August 17, 2013 (including the days of Pattern C) and from August 30, 2013 to September 12, 2013 (including the days of Pattern A). Fig. 20 shows the land use data input (Domain 2). In this simulation condition, "urban" is one land use category that is further classified into three categories because of the use of the urban canopy model (UCM) (Kusaka, Kondo, Kikegawa, & Kimura, 2001; Vitanova & Kusaka, 2018) on the surface scheme. Concerning the method used in that classification, the area ratios of each category "high building," "low-densely building," "low building" and "non-urban" are calculated in the mesh (Domain 2). Next, "urban" is classified into three categories based on the cluster analysis result using those area ratios as variables. In the next section, analyses are performed that target Domain 2 and use the data from August 10 to August 16 (Pattern C) and September 5 (Pattern A).

4.2.2. Validation and outline of simulation results

First, in order to confirm the calculations' accuracy, a comparison of the simulation results and observed data was performed on temperature and wind speed using the hourly value in air pollution monitoring stations and the Hiroshima Meteorological Observatory. Specifically, the comparison of temperature and wind speed was conducted using three indexes: bias, RMSE and correlation. The results are shown in Table 9.

$$(\text{Bias}) = \frac{1}{N}\sum_{i=1}^{N} u_{yi} - \frac{1}{N}\sum_{i=1}^{N} u_{xi} \tag{6}$$

$$(\text{RMSE}) = \sqrt{\frac{1}{N}\sum_{i=1}^{N} (u_{yi} - u_{xi})^2} \tag{7}$$

$$(\text{Correlation}) = \frac{1}{N}\sum_{i=1}^{N} (u_{xi} - \overline{U_x})(u_{yi} - \overline{U_y})/\sigma_X \sigma_Y \tag{8}$$

(N: sample size; u_{xi}: observed value; u_{yi}: calculated value; $\overline{U_x}$: the average of observed values; $\overline{U_y}$: the average of calculated values; σ_X: the standard deviation of observation value; σ_Y: the standard deviation of

Table 7
The criteria of wind blowing pattern sub classification and results.

Wind pattern	Criteria	Classification result
Pattern C-1 The wind from coast in a rush (18 days)	Wind from the coast at a velocity of 1 [m/s] or greater blows in all 3 points after blowing wind from the coast at a velocity of 1 [m/s] or greater within one hour in coastal area (Inokuchi).	July 20, July 21, July 22, July 26, Aug. 6, Aug. 7, Aug. 8, Aug. 10, Aug. 13, Aug. 15, Aug.16, Aug. 17, Aug. 18, Aug. 19, Aug. 20, Aug. 21, Sep.19, Sep. 20
Pattern C-2 The wind from coast gradually (11 days)	Wind from the coast at a velocity of 1 [m/s] or greater blows in all 3 points after blowing wind from the coast at a velocity of 1 [m/s] or greater for more than two hours in coastal area (Inokuchi).	Aug. 11, Aug. 12, Aug.14, Aug. 27, Aug.28, Sep. 10, Sep. 13, Sep. 14, Sep.21, Sep. 22, Sep. 23

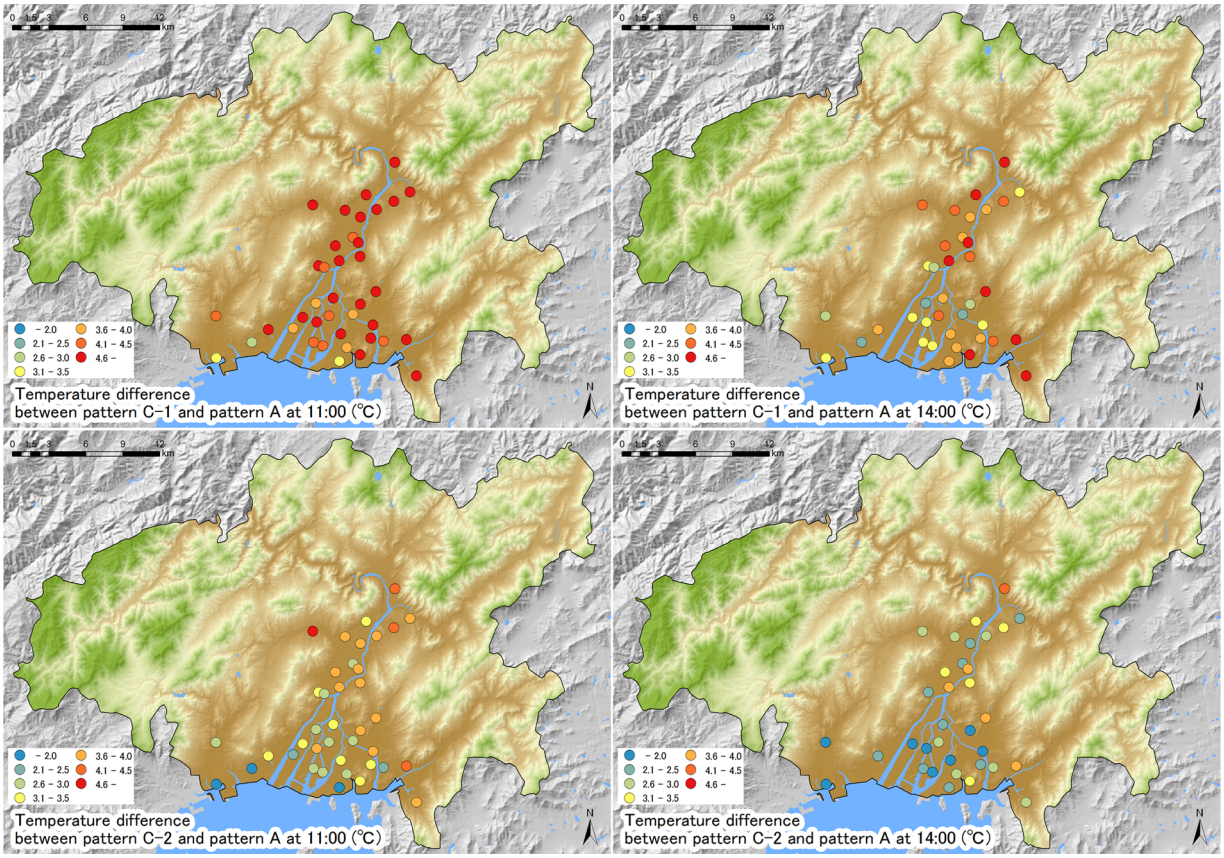
Temperature difference
between pattern C-1 and pattern A at 11:00 (℃)
Temperature difference
between pattern C-1 and pattern A at 14:00 (℃)
Temperature difference
between pattern C-2 and pattern A at 11:00 (℃)
Temperature difference
between pattern C-2 and pattern A at 14:00 (℃)

Fig. 16. The sea breeze effect at 11:00 and 14:00 in each pattern (C-1 and C-2).

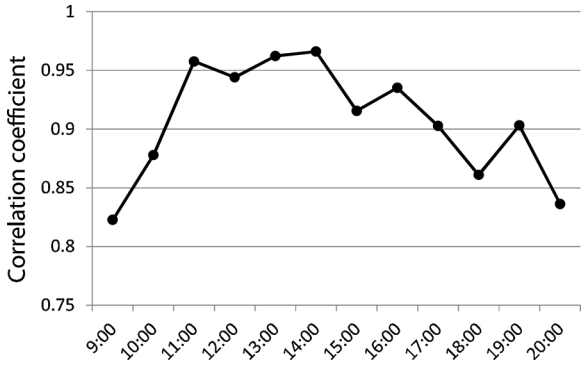

Fig. 17. The hourly correlation coefficient of the sea breeze effect between pattern C-1 and pattern C-2 from 9:00 to 20:00.

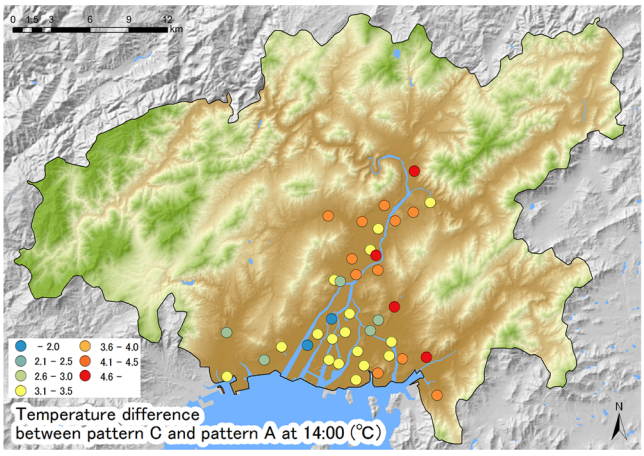

Fig. 18. The map of hourly sea breeze effect was constructed by using all of the data of pattern C (14:00).

calculation value).

The comparison of wind that arose from 7:00 to 18:00 was made at seven observation points (Fig. 21). According to these comparisons, the difference between simulation results and observed data is small.

Next, the temperature distribution at 2 m height and the wind distribution at 10 m height at 14:00 on August 13 and September 5 are shown in Fig. 22 as an example. According to these results, it can be seen that the temperature in coastal areas is low, but in inland areas it is high on August 13, and the prevailing sea breezes blow throughout the whole plains area. On the other hand, from the results of September 5, it can be seen that the temperature difference within the plains area is smaller than that on August 13, although the temperature in coastal areas is slightly high and the prevailing wind from the north blows throughout the whole plains area.

4.2.3. Making the map of sea breeze effect distribution

The mesh of the plains area (Fig. 8), which is defined in Section 3.1., was targeted. The hourly sea breeze effect (the temperature difference between Pattern C and Pattern A) was calculated and mapped. The results at 11:00 and 14:00 are shown as examples in Fig. 23. The sea breeze effect is relatively larger in the coastal area and smaller in the inland area. Therefore, the hourly correlation coefficients between the sea breeze effect of Pattern C based on the observed temperature and that based on numerical simulation results are overlapped with the observation points (Fig. 24). Also, each relationship at 11:00 and 14:00 is shown in Fig. 25. From these results, it is apparent that the spatial distribution pattern of sea breeze effects made from the numerical calculation is similar to the one made from the observed temperatures.

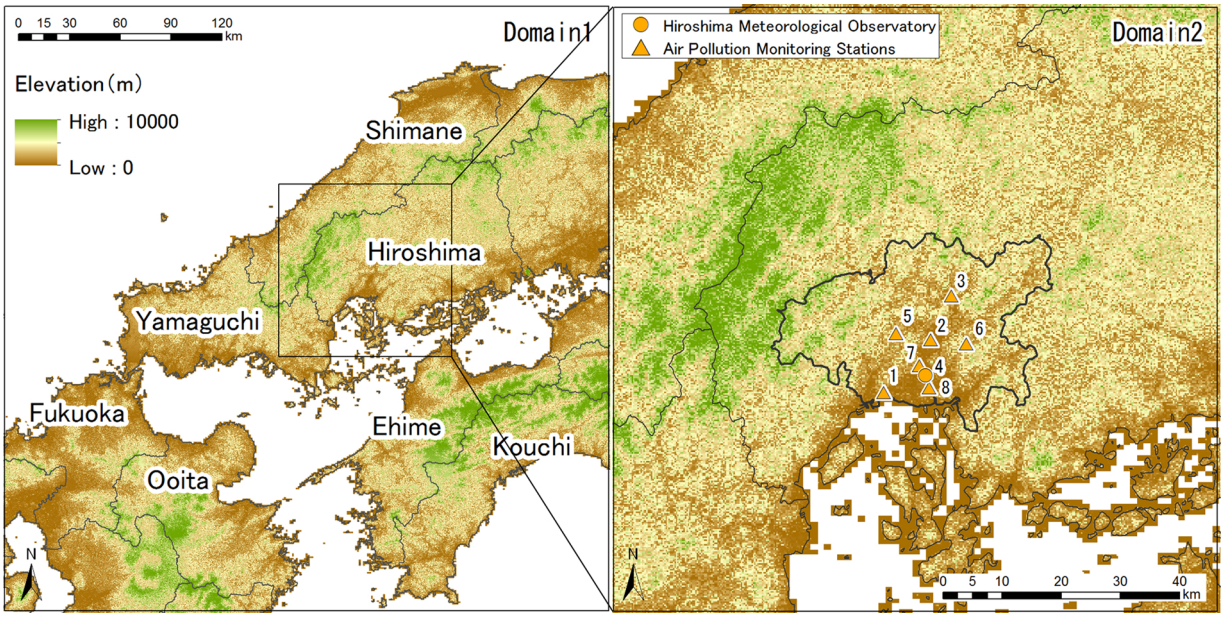

Fig. 19. The calculation domains which are defined for WRF and the location of Hiroshima Meteorological Observatory and seven air pollution Monitoring Stations.

Therefore, in the following subsection, factor analysis of the hourly sea breeze effect is conducted using these simulation results.

4.2.4. The relationship between temperature distribution and wind speed distribution

In all meshes in which the mesh number is 127 within the plains area, the correlation coefficient between the hourly average temperature and wind speed of Pattern C is calculated by confirming that the sea breeze effect can be shown by the calculated value of the wind speed. According to the results, shown in Fig. 26, the correlation coefficient between temperature and wind speed is not high but is particularly low until 13:00. The effect of sea breezes on mitigating urban warming is small in inland areas at 11:00 because this wind seems to be different from the sea breezes. As a result, it is difficult to make the map of sea breeze effect distribution based on the wind speed distribution in the plains area.

4.2.5. The difference of sensible heat advection by area

The result of the last subsection confirms that the relationship between temperature distribution and wind speed distribution is small. Therefore, this subsection describes the factor analysis of sea breeze effect by using hourly sensible heat advection by using previous study as a reference (Takane, Ohashi, Kusaka, Shigeta, & Kikegawa, 2013).

First, the hourly sensible heat advection on August 13 (a representative day of C-1) and August 12 (a representative day of C-2) was calculated on three representative meshes (Fig. 23). Specifically, the net heat input into the atmospheric mixed column (sensible heat storage), $Q_c(SH)$, and the time-integrated sensible heat flux from the ground surface, $Q_g(SH)$, were calculated in each mesh by using simulation results based on a previous study (Ishida, Munehiro, Matsusita, & Horikoshi, 2013). Also, the sensible heat advection, $Q_{adv}(SH)$, was calculated using these calculation results. The calculation condition is shown in Table 10.

The calculation results of each mesh are shown in Fig. 27. With respect to the results of Pattern C-1 and Pattern C-2, the absolute value

Table 8
The calculation condition of WRF.

Period		August 4-17, 2013 (Spin up time: August 4-9) August 30-September 12, 2013 (Spin up time: August 30-Spetember 4) (Separate Calculation)
Vertical grid		28 layers (Surface ~100hPa)
Horizontal grid		Domain1:3km dimension 120*120, Domain2: 1kmdimension 103*103 (Staggered Model Grid, 2-way nesting)
Meteorological data		Meteorological Agency Meso Objective Analysis Data (every 3 hour, 10km grid, 20 layers) NCEP Re-analysis global objective analysis data (every 6 hour, 1° Grid,17 layers)
Land data	Elevation	Numerical Map (Resolution about 250)
	Land cover	Digital National Land Information (Resolution about 100) Land cover mesh data in urban area of Digital National Land Information (Resolution about 100) Building use data of Basic Surveys Concerning City Planning in Hiroshima city Data collection of Arc GIS (Esri Japan Corporation) Actual vegetation map of Ministry of the Environment
Microphysics		Purdue Lin scheme
Radiation	Long wave	Rapid Radiative Transfer Model (RRTM)Longwave
	Short wave	MM5(Dudhia)Shortwave
PBL scheme		Mellor-Yamada-Janjic PBL
Surface scheme	Urban area	Urban Canopy Model(UCM)
	Nonurban area	Noah LSM
Cumulus parameterization		None
FDDA		None

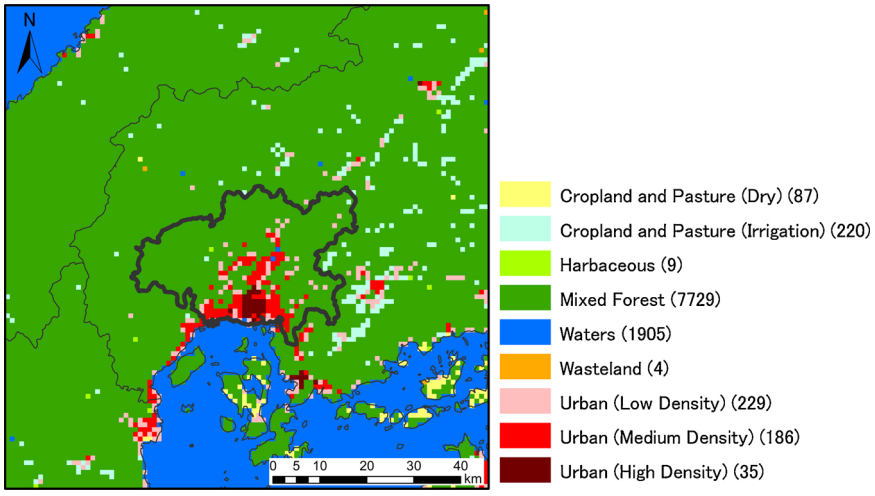

Fig. 20. The land cover data. The number of meshes is in parenthesis.

of sensible heat advection in the coastal area (mesh A) is relatively larger at all times. This is because the sea breeze effect is relatively larger. Also, the sensible heat advection in the middle area (mesh B) is large at 12:00, while in the inland area (mesh C), it is large at 16:00. This is because the sea breeze reaches the inland area gradually. In addition, blowing wind in the inland area does not have the effect of mitigating urban warming because of the absolute value of sensible heat advection in the morning in the inland area. As for the results of Pattern A, the absolute value of sensible heat advection in all meshes is smaller than that of Pattern C-1 and C-2. It was assumed that the blowing wind in Pattern A days does not have the same effect of mitigating urban warming as the sea breeze.

According to the above results concerning the sea breeze effect, the temperature difference between Pattern C and Pattern A is formed by sea breezes.

4.2.6. Analyzing the relationship between the observed temperature and the surrounding ventilation condition

The temperature in each place is influenced not only by the sea breeze effect, which is a regional factor, but also by the surrounding ventilation condition, which is the local factor. Therefore, in this subsection, an analysis of the relationship between the observed temperature (14:00) and the surrounding ventilation condition is performed by using RBB in the direction of south-southwest.

First, the plains area was classified into the following two zones: 1) the area that is influenced by sea breezes (zone L), and 2) the area that is not influenced by sea breezes (zone S). The boundary temperature value is 6.5 °C. As a result, 20 observation points were classified in zone L, while 19 observation points were classified in zone S. Next, the correlation coefficient between these RBB and average temperature at 14:00 from August 10 to August 16 was calculated for each observation (Fig. 28). These days are within the calculation period and have also been classified in Pattern C. Also, as with the RBB, the combination of r = 100 m and h = 5 m was used (the correlation coefficient where temperature is highest in daytime). According to this figure, a positive correlation coefficient can be seen between temperature at 14:00 and RBB in zone L but such a tendency cannot be seen in zone S. The higher the RBB in the direction south-southwest becomes, the higher the temperature becomes in the south plains area where the sea breeze effect is. However, the influence of RBB on the temperature is relatively small in the north plains areas. From these results, it is apparent that there are areas for which countermeasures for mitigating ventilation condition such as building planning arrangements are effective and areas for which it is not effective. In Hiroshima, the effect is large in the south plain area. The fluctuation of correlation coefficients also depends on the days' results due to the difference in wind strength or the like. In the future, an analysis related to this consideration will be undertaken.

5. Evaluating the factors of temperature distribution comprehensively in mountain areas

In this chapter, understanding the summer temperature distribution and evaluating its factors comprehensively were undertaken using 15

Table 9
(a) The results comparison of the simulation results and observed data (temperature). (b) The results comparison of the simulation results and observed data (wind speed)

Observation Point		Bias (°C)	RMSE (°C)	Correlation
Air Pollution Monitoring Station	3	0.13	1.78	0.92
	7	−0.57	1.13	0.92
Hiroshima Meteorological Observatory	4	−0.15	0.93	0.96

Observation Point		Bias (m/s)	RMSE (m/s)	Correlation
Air Pollution Monitoring Station	1	−0.23	0.81	0.83
	2	0.47	1.20	0.52
	3	0.35	1.10	0.53
	5	−0.27	1.11	0.54
	6	0.06	0.85	0.67
	7	−0.82	1.35	0.55
	8	−0.28	1.05	0.56

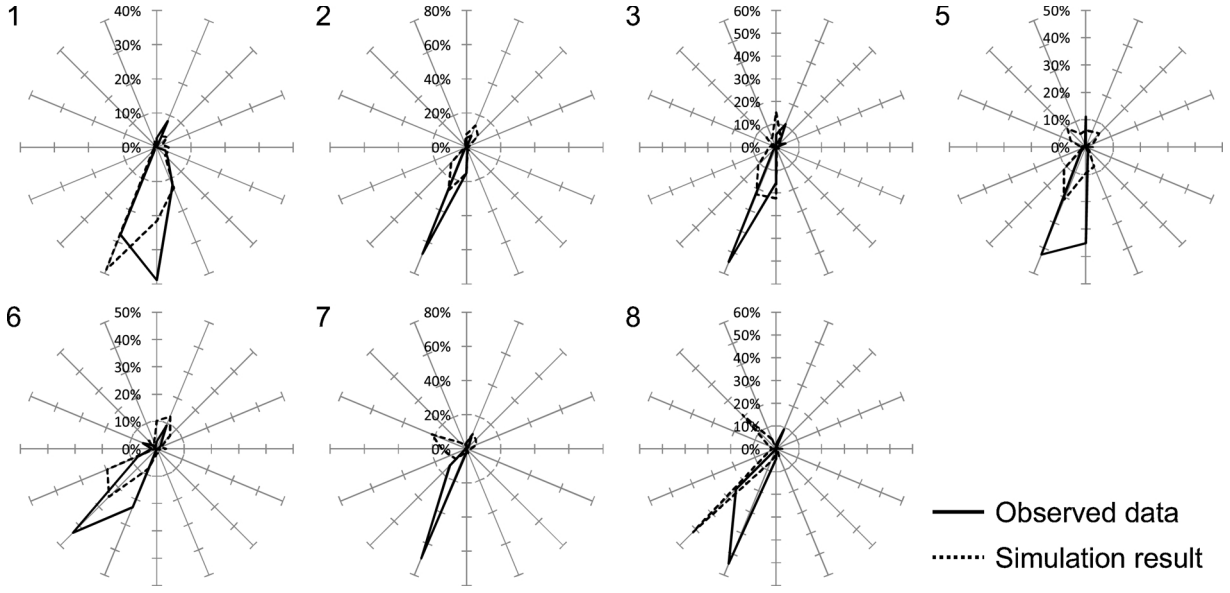

Fig. 21. The comparison of wind that arose from 7:00 to 18:00 was made at seven observation points.

observation points in the mountain areas (Fig. 7). Typical fine-weather summer days (29 days), extracted in the preceding chapter, were targeted as the temperature data. The factors of temperature distribution include 1) amount of insolation, 2) topographic position index (TPI), 3) surrounding green areas, and 4) amount of cold air targeted by using previous studies as a reference (Ishida et al., 2013; Noguchi et al., 2014; Ogawa et al., 2011). Also, 3) is similar to the factors in Chapter 3.

5.1. Outline of temperature distribution factors

5.1.1. Amount of insolation

The hourly amount of insolation was calculated using the elevation data (Geospatial Information Authority of Japan: Digital Map 50 m Grid) on GIS on typical fine-weather summer days. In addition, it was calculated as global solar radiation. The solar orbit of each day was calculated and each hourly amount of insolation from 6:00 to 17:00 was

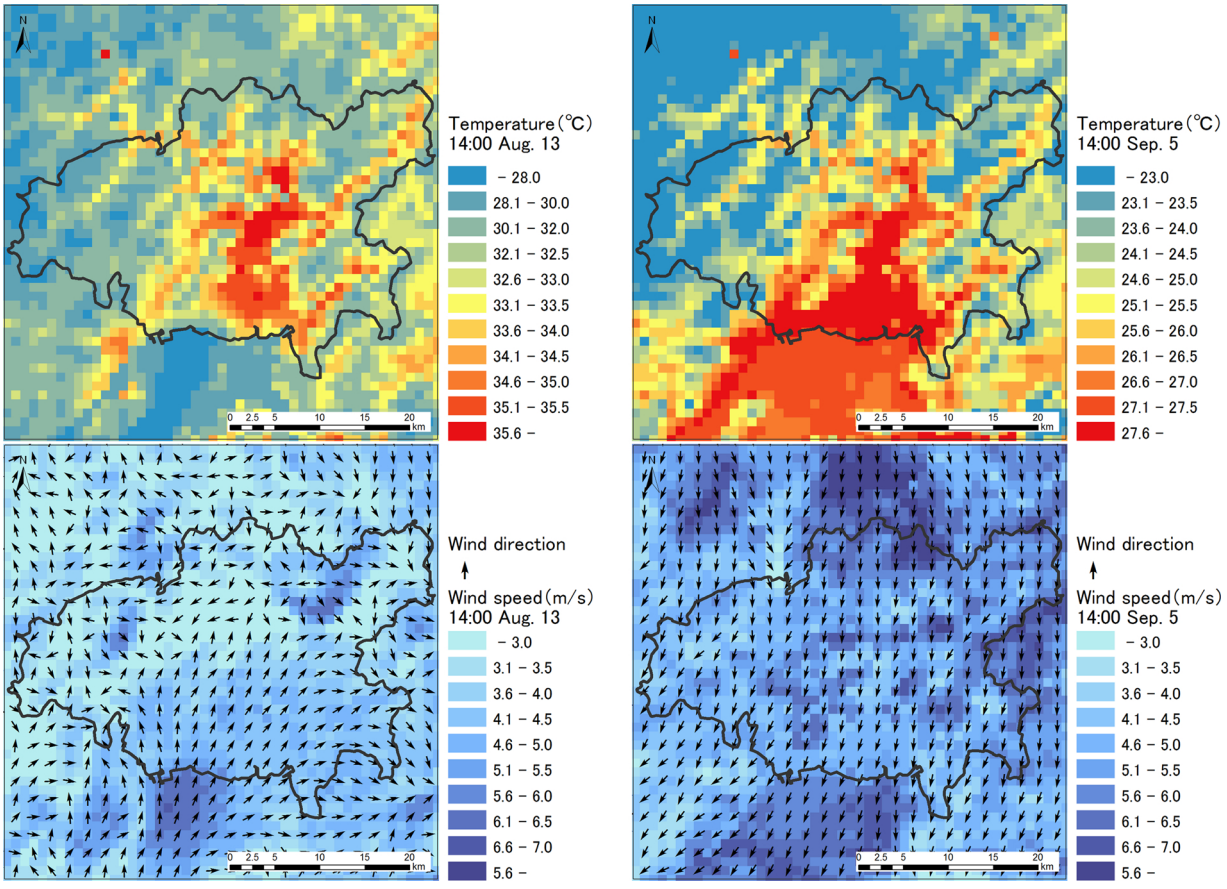

Fig. 22. The simulation results of the temperature distribution at 2 m height and the wind distribution at 10 m height at 14:00 on August 13 and September 5.

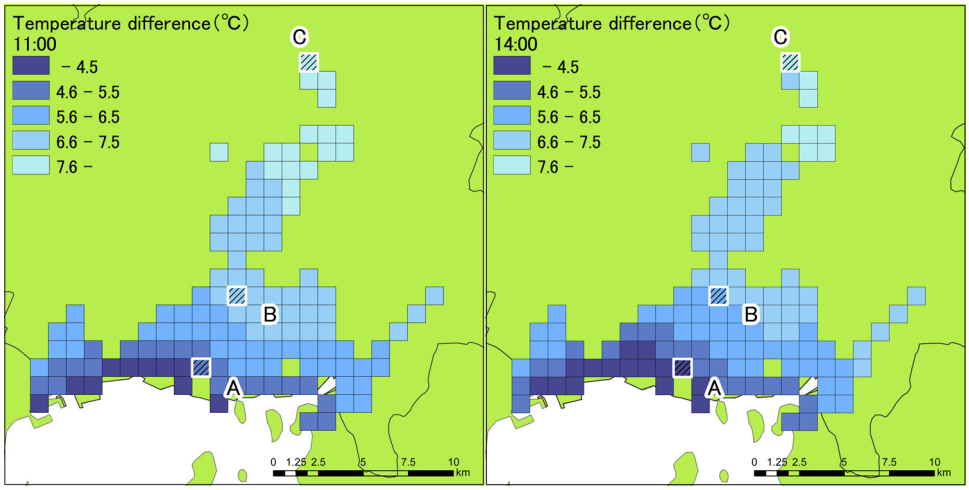

Fig. 23. The hourly sea breeze effect distribution at 11:00 and 14:00 by simulation results. The mesh A, B and C show the representative meshes for analysis of the difference of sensible heat advection by area.

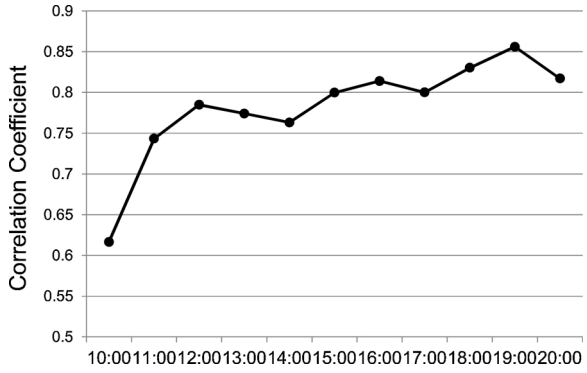

Fig. 24. The hourly correlation coefficients between the sea breeze effect of pattern C based on the observed temperature and that based on numerical simulation results are overlapped with the observation points from 10:00 to 20:00.

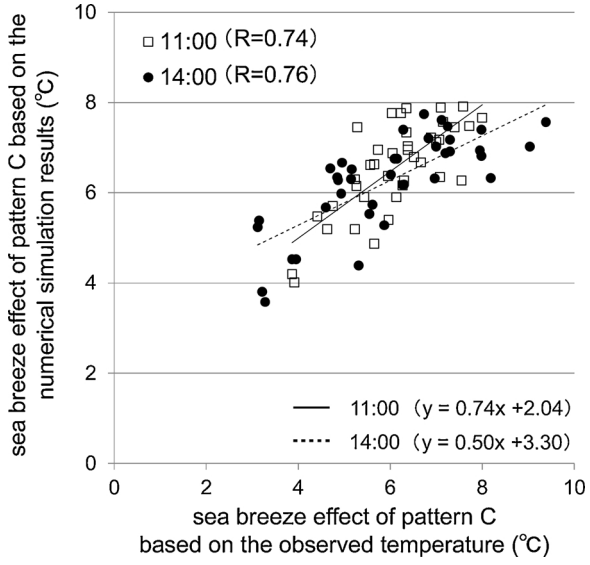
sea breeze effect of pattern C based on the numerical simulation results (℃)
□ 11:00 (R=0.74)
● 14:00 (R=0.76)
11:00 (y = 0.74x +2.04)
14:00 (y = 0.50x +3.30)
sea breeze effect of pattern C based on the observed temperature (℃)
0 2 4 6 8 10

Fig. 25. The correlation coefficients between the sea breeze effect of pattern C based on the observed temperature and that based on numerical simulation results are overlapped with the observation points at 11:00 and 14:00.

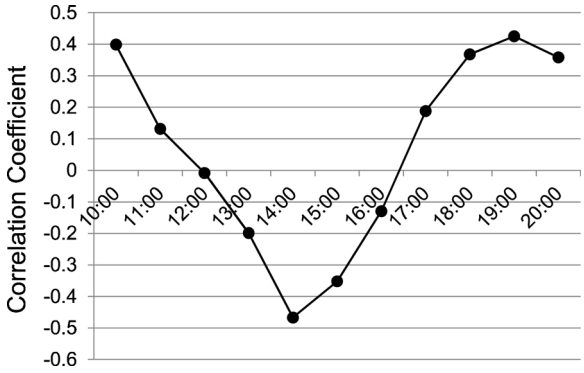

Fig. 26. The correlation coefficient between the hourly average temperature and wind speed of pattern C.

Table 10
The calculation condition of the sensible heat advection.

The formula	$Q_c(SH) = \int_{Zg}^{Ztop} c_p\rho(\theta_N - \theta_{N-1})dz \cdots$(a) $Q_g(SH) = SH_N \cdots$(b) $Q_{adv}(SH) = Q_c(SH) - Q_g(SH) \cdots$(c) ($SH$: Sensible heat flux from the ground surface [MJ/m^2]; cp: Specific heat at constant pressure of air [J/kg· K]; ρ: Air density [kg/m^3]; θ: Potential temperature [K]; Zg: Elevation [m]; $Ztop$: Top elevation of atmospheric mixed column [m]; N: time)
[Top elevation of atmospheric mixed column]	The top elevation of the atmospheric mixed column was defined by using the potential temperature vertical distribution that is made from the simulation results. First, the potential temperature difference between atmospheric layers from the lowest layer was confirmed. Next, the height up to that difference of more than 1 K was initially defined as the top elevation of the atmospheric mixed column. From this result, it was clear that the average value of the top elevation of the atmospheric mixed column was about 1025 m. Also, according to the observed data in the plains area, at Hiroshima-Nishi Airport, it was confirmed that the difference is not large between that average value of the top elevation of the atmospheric mixed column and the clouds' average height in daytime in summer (about 1066 m).

calculated on typical fine-weather summer days using those results. The result at 13:00 on August 12 is shown in Fig. 29 as an example. Next, the integration of hourly amounts of insolation was calculated from sunrise on each of the 29 days, and those hourly average integrated values were defined as the index of the amount of insolation (AI). In

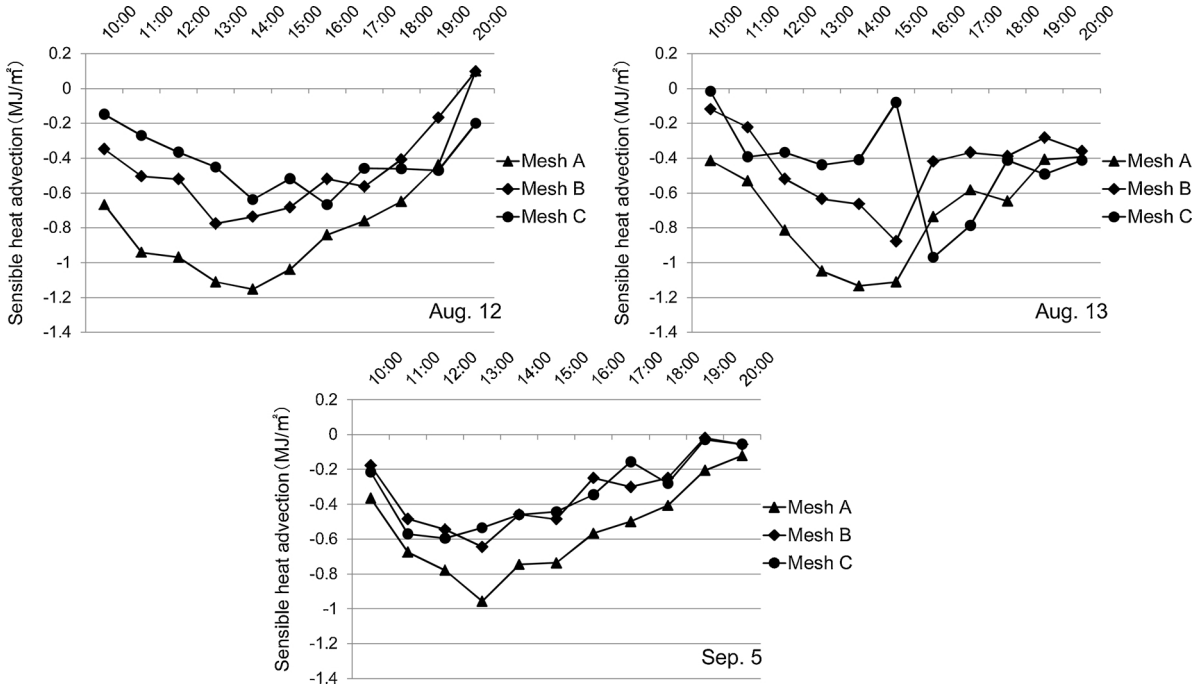

Fig. 27. The calculation results of sensible heat advection of each mesh.

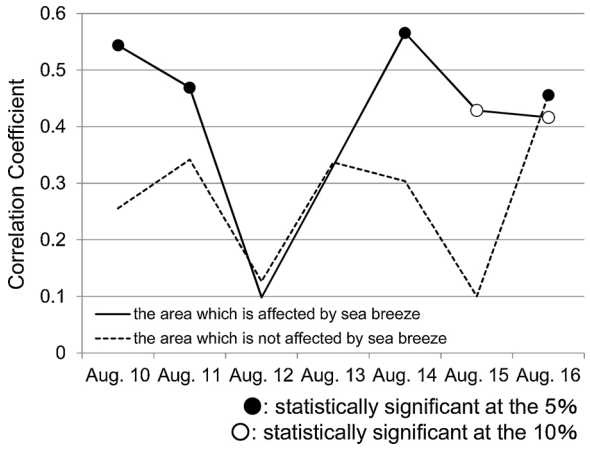
Correlation Coefficient
the area which is affected by sea breeze
the area which is not affected by sea breeze
Aug. 10 Aug. 11 Aug. 12 Aug. 13 Aug. 14 Aug. 15 Aug. 16
●: statistically significant at the 5%
○: statistically significant at the 10%

Fig. 28. The correlation coefficient between these RBB and average temperature at 14:00 from August 10 to August 16.

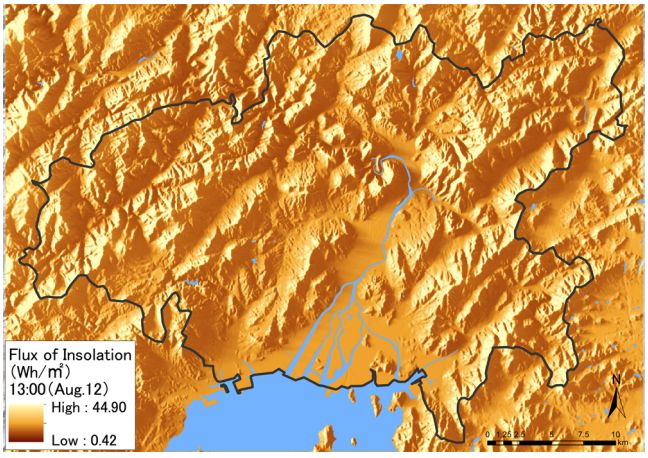

Fig. 29. The amount of insolation at 13:00 on August 12.

addition, only terrain was considered, while detailed factors such as buildings or trees were not considered in this calculation of global solar radiation. This is because much of the solar energy received by the surfaces of buildings or trees is released into the air finally and also affects the air temperature rises (Narumi, Habara, & Mizuno, 2009).

5.1.2. *Topographic position index (TPI)*

In this subsection, TPI was calculated to clear the influence of geographical features on temperature surrounding observation points by using elevation data similar to that in the above subsection. TPI is defined as the index representing the relative unevenness of geography (Tanaka, Mikasa, Uchihira, Yamazaki, & Shigemura, 2014). Specifically, TPI represents the differences between the elevation value of the cell overlaid with each observation point and the average elevation value of the cell surrounding it, which is calculated by the formula (9). The outline of TPI is also shown in Fig. 30.

$$TPI = X - Y \tag{9}$$

(X: the elevation value of a cell overlaid with each observation point; Y: average elevation value of cell surrounding each observation point)

The high value of TPI represents the elevation of observation that is higher than the others when the observation point is located in the surrounding ridge of mountains. On the other hand, the low value of TPI represents the elevation of observation that is lower than the others when the observation point is located in the surrounding mountain valley. Y shows the average elevation value within the circle at the

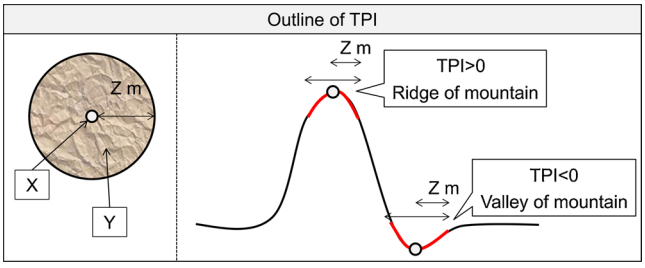

Fig. 30. The conceptual diagram of TPI (Topographic Position Index).

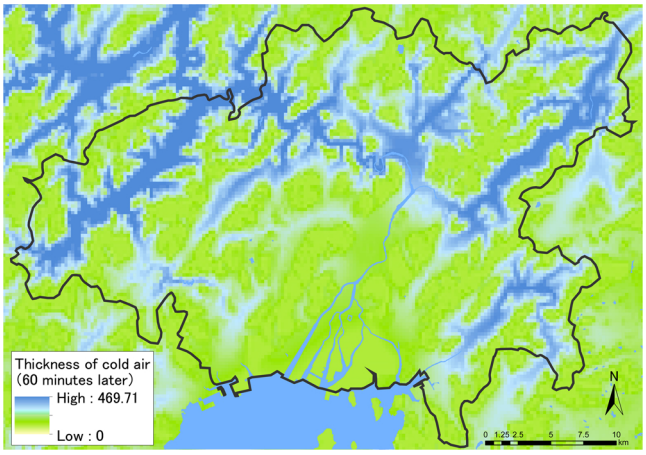

Fig. 31. The simulation results of the thickness of cold air.

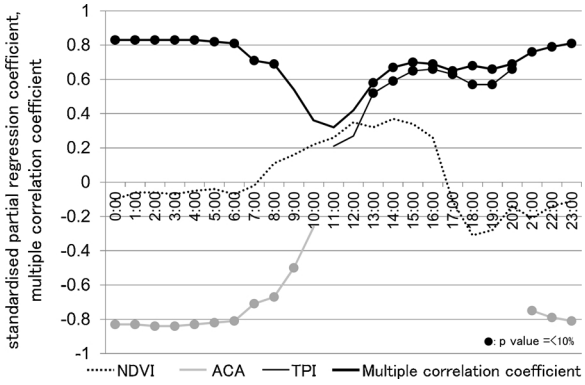

Fig. 32. The hourly standard partial regression coefficient and multiple correlation coefficient (Mountain area).

center of the cell overlaid with the observation point. The radius of the circle is defined as 1300 m, because the correlation coefficient between average temperature and TPI, which is calculated with the radius of 1300 m, is highest from 100 m to 2000 m every 100 m.

5.1.3. Amount of cold air

In this subsection, the fill and outflow processes of cold air are simulated by numerical calculation using a shallow water model, and the result, the amount of cold air (ACA) is defined as one of the factors. The shallow water model is the applied model of the shallow water equation (Takebayashi & Moriyama, 2002). In this study, the shallow model made in the previous study was revised to consider the influence of land use. As for the concrete calculation process, the cold air that is generated by the parameter for cold air potential "q" starts to flow from the condition wherein the ACA is zero and it is flowing down over time under the influence of elevation and resistance "c." In this calculation, it is necessary to prepare the elevation data and define the values of "q" and "c." The elevation data are similar to the above subsections, and "q" and "c" are defined using previous studies (Takebayashi & Moriyama, 2002; Takebayashi, Akagawa, & Moriyama, 2010). In addition, "q" is defined separately by dividing the targeted area into "urban" and "non-urban" using land cover data. The results 60 minutes later are shown in Fig. 31. From these results, it can be seen that, over time, ACA in the valley is large; that is to say, the fill and outflow processes of cold air are sufficiently represented.

5.2. Comprehensive evaluating using multiple regression analysis

In this section, multiple regression analysis was performed to comprehensively evaluate the influence of factors on temperature. Table 11 shows the correlation coefficient between the explanatory variables. As for AI, the correlation coefficients between hourly amounts of insolation and the others were also calculated because they are different each time. From this table, it can be seen that AI is related to the other three variables and TPI is related to ACA. Therefore, TPI, NDVI-300, and ACA were defined as explanatory variables. Regarding the TPI and ACA, the larger correlation coefficient (absolute value) with hourly average temperature was selected each time as follows: the explanatory variables from 0:00 to 10:00 and from 20:00 to 23:00 are defined as ACA, while those from 11:00 to 20:00 are defined as TPI.

The hourly standard partial regression coefficient and multiple correlation coefficient are shown in Fig. 32. First, the multiple correlation coefficients were as high as 0.6 to 0.8 from 0:00 to 8:00 and from 13:00 to 23:00; then this multiple regression equation was used to explain objective variables with a determination coefficient of around 0.3 to 0.6 in these time ranges. The standard partial regression coefficient, TPI, was high in a positive direction in daytime. From this result, it was assumed that the daytime summer temperature in mountain areas had increased due to the surrounding geographical features namely, AI. In addition, the standard partial regression coefficient of ACA was high in a negative direction at night. From these results, it can be assumed that the temperature at night had reduced due to the cold air drainage or cold air lakes. As for NDVI-300, the standard partial regression coefficient was relatively low in the plains area. This is because the influence of the AI or ACA from surrounding geographical features is larger than that of the surrounding green area in mountain areas, which is often rich. Also, the standard partial regression coefficient and multiple correlation coefficient were relatively low from 9:00 to 12:00. This is because temperature increases in the surrounding area are not

Table 11
The correlation coefficients among the explanatory variables (mountain area).

	AI6:00	AI7:00	AI8:00	AI9:00	AI10:00	AI11:00	AI12:00	AI13:00	AI14:00	AI15:00	AI16:00	AI17:00	TPI	NDVI	ACA
AI 6:00	***1.00***	***0.98***	***0.95***	***0.88***	***0.79***	***0.65***	0.47	0.25	0.02	−0.18	−0.35	−0.40	***−0.76***	0.11	***0.61***
AI 7:00	***0.98***	***1.00***	***0.98***	***0.94***	***0.87***	***0.75***	0.59	0.37	0.13	−0.08	−0.26	−0.31	***−0.75***	0.22	0.59
AI 8:00	***0.95***	***0.98***	***1.00***	***0.98***	***0.93***	***0.84***	***0.70***	0.51	0.28	0.05	−0.13	−0.18	***−0.71***	0.33	0.53
AI 9:00	***0.88***	***0.94***	***0.98***	***1.00***	***0.98***	***0.92***	***0.81***	***0.64***	0.43	0.21	0.02	−0.03	***−0.63***	0.43	0.45
AI 10:00	***0.79***	***0.87***	***0.93***	***0.98***	***1.00***	***0.97***	***0.90***	***0.77***	0.58	0.38	0.19	0.13	−0.53	0.53	0.33
AI 11:00	***0.65***	***0.75***	***0.84***	***0.92***	***0.97***	***1.00***	***0.97***	***0.88***	0.73	0.56	0.38	0.32	−0.39	***0.62***	0.18
AI 12:00	0.47	0.59	***0.70***	***0.81***	***0.90***	***0.97***	***1.00***	***0.96***	***0.87***	***0.73***	0.57	0.52	−0.21	***0.67***	0.01
AI 13:00	0.25	0.37	0.51	***0.64***	***0.77***	***0.88***	***0.96***	***1.00***	***0.96***	***0.87***	***0.75***	***0.71***	0.00	***0.68***	−0.18
AI 14:00	0.02	0.13	0.28	0.43	0.58	***0.73***	***0.87***	***0.96***	***1.00***	***0.97***	***0.89***	***0.86***	0.20	***0.63***	−0.37
AI 15:00	−0.18	−0.08	0.05	0.21	0.38	0.56	***0.73***	***0.87***	***0.97***	***1.00***	***0.97***	***0.95***	0.38	0.55	−0.52
AI 16:00	−0.35	−0.26	−0.13	0.02	0.19	0.38	0.57	***0.75***	***0.89***	***0.97***	***1.00***	***0.99***	0.53	0.42	***−0.65***
AI 17:00	−0.40	−0.31	−0.18	−0.03	0.13	0.32	0.52	***0.71***	***0.86***	***0.95***	***0.99***	***1.00***	***0.57***	0.38	***−0.67***
TPI	***−0.76***	***−0.75***	***−0.71***	***−0.63***	−0.53	−0.39	−0.21	0.00	0.20	0.38	0.53	0.57	***1.00***	−0.09	***−0.85***
NDVI	0.11	0.22	0.33	0.43	0.53	***0.62***	***0.67***	***0.68***	***0.63***	0.55	0.42	0.38	−0.09	***1.00***	−0.09
ACA	***0.61***	0.59	0.53	0.45	0.33	0.18	0.01	−0.18	−0.37	−0.52	***−0.65***	***−0.67***	***−0.85***	−0.09	***1.00***

influenced by AI from 9:00 to 10:00 and the difference in AI is small when the altitude of the sun is high from 11:00 to 12:00. However, it is necessary to address this point in the future.

6. Climate zoning and making UECMs

In this chapter, climate zoning and construction of UECMs are performed using the results from Chapters 3 to 5. From these results, it can be said that the influence of "DCDS" and "RBB-SSW" is large in the plains area, while that of "TPI" is large in the mountain areas during daytime. On the other hand, at night, the influence of "DCDS," "NDVI-300," and "RBB-NNW" is large in the plains area and that of "ACA" is large in the mountain areas. Therefore, each threshold value is defined by the relationship between those factors and average temperature, and zoning is performed on the basis of each value by using GIS. The concrete zoning methods are shown in the following section at daytime and at night.

6.1. Zoning at daytime

For zoning in the plains area, the area is first gradually classified into three zones using the threshold based on the regression equation between "DCDS" and the average temperature data of typical fine-weather summer days (29 days): ZONE 5, ZONE 6, and ZONE 7 (Fig. 33). Next, zoning is undertaken using the threshold of "RBB-SSW." In this classification, it takes an enormous amount of time to calculate the RBB distribution in three dimensions throughout the whole plains area. Therefore, a calculation method of RBB distribution in two dimensions was devised, and this zoning was performed by using the threshold defined by the relationship between temperature and "RBB in two dimensions." It is also known that the correlation coefficient between "RBB-SSW in two dimensions" and "RBB-SSW in three dimensions" is large. As for the specific classification, the correlation coefficients between the average temperatures in observations where DCDS was less than X km and "RBB-SSW in two dimensions" were calculated in ascending order because there were areas where the correlation coefficients between temperature and "RBB-SSW" are relatively large, and areas where these were relatively small in the plains area. From these results, the correlation coefficient between the temperatures in 10 observations is where X is 3 and "RBB-SSW in two dimensions" is the largest. Therefore, the threshold was defined using the relationship between the average temperatures and "RBB-SSW in two dimensions," and the zoning was performed using that threshold. In addition, the zoning result is only shown in Zone 5 where the sea breeze blows the most in the plains area (Fig. 33).

As for the zoning in the mountain area, the area is gradually classified into three zones using the threshold of "TPI": Zone 1, Zone 2, and Zone 3 (Fig. 33).

6.2. Zoning at night

As for the zoning in the plains area, the area was first gradually classified into three zones using the threshold based on the regression equation between "NDVI-300" and the average temperature data of typical fine-weather summer days (29 days): Zone 4, Zone 5, and Zone 6 (Fig. 34). Next, the plains area was gradually classified into two zones using the threshold of "DCDS": Zone 8 and Zone 9 (Fig. 34). Finally, zoning was conducted using the threshold of "RBB-NNW." In the same

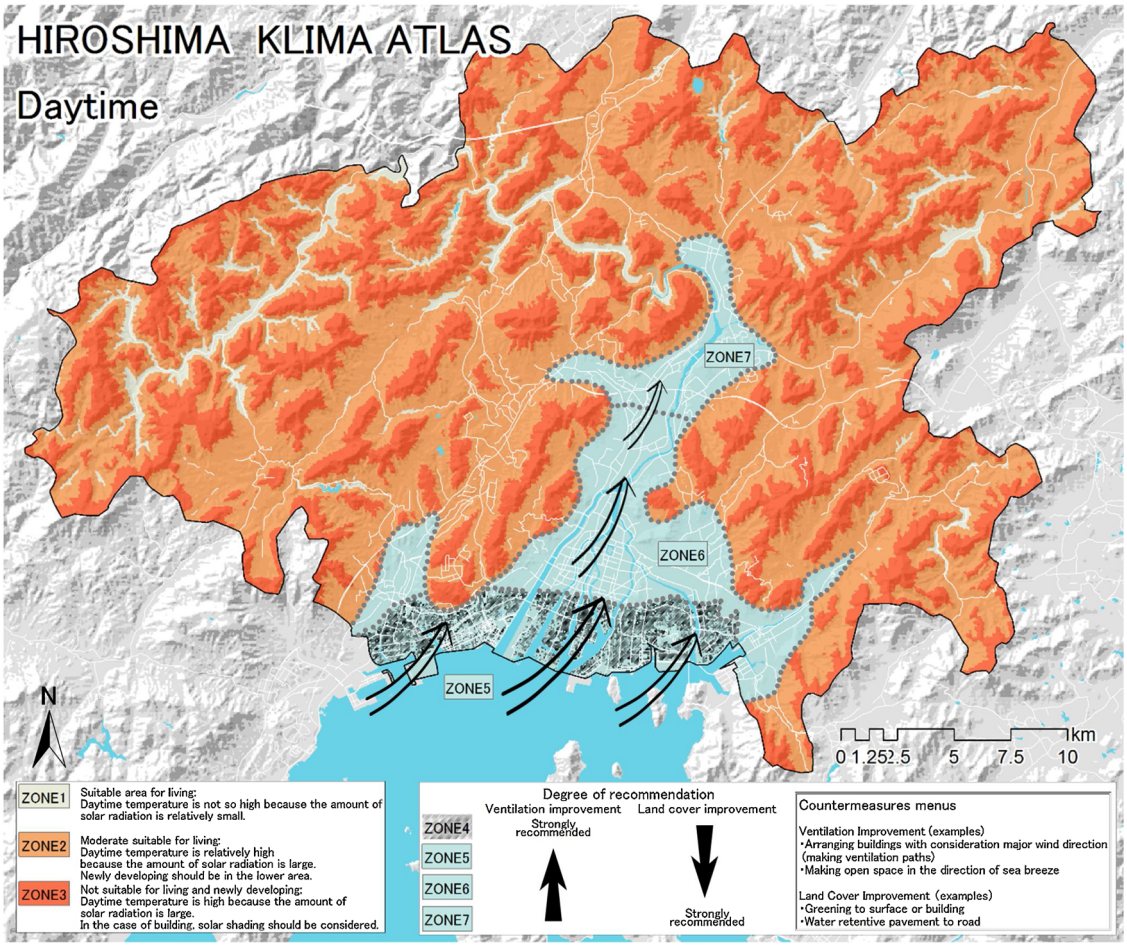
HIROSHIMA KLIMA ATLAS
Daytime
ZONE7
ZONE6
ZONE5
N
km
0 1.252.5 5 7.5 10
ZONE1 Suitable area for living:
Daytime temperature is not so high because the amount of solar radiation is relatively small.
ZONE2 Moderate suitable for living:
Daytime temperature is relatively high because the amount of solar radiation is large.
Newly developing should be in the lower area.
ZONE3 Not suitable for living and newly developing:
Daytime temperature is high because the amount of solar radiation is large.
In the case of building, solar shading should be considered.
Degree of recommendation
Ventilation improvement
Land cover improvement
ZONE4
ZONE5
ZONE6
ZONE7
Strongly recommended
Strongly recommended
Countermeasures menus
Ventilation Improvement (examples)
·Arranging buildings with consideration major wind direction (making ventilation paths)
·Making open space in the direction of sea breeze
Land Cover Improvement (examples)
·Greening to surface or building
·Water retentive pavement to road

Fig. 33. Urban Climate Environmental Map at daytime.

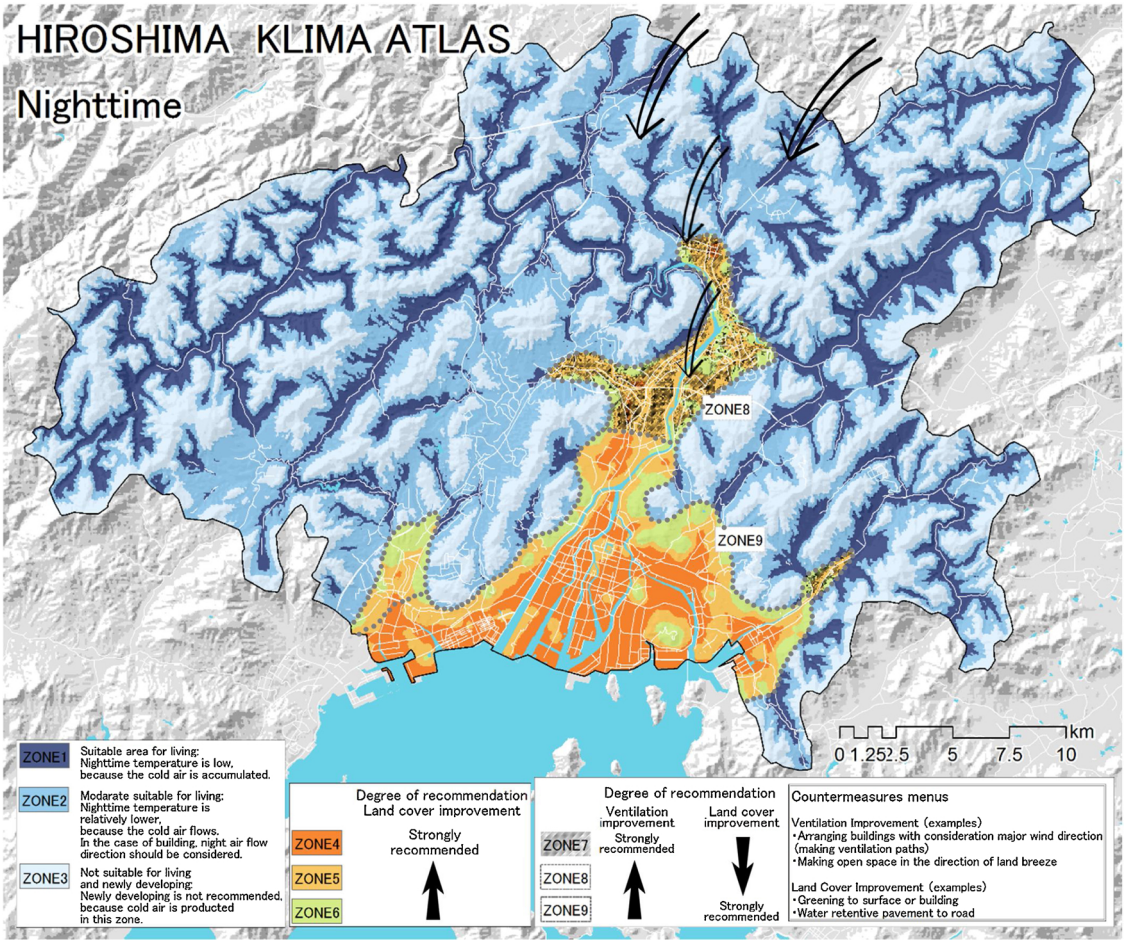
HIROSHIMA KLIMA ATLAS
Nighttime
ZONE8
ZONE9
km
0 1.252.5 5 7.5 10
ZONE1 Suitable area for living: Nighttime temperature is low, because the cold air is accumulated.
ZONE2 Modarate suitable for living: Nighttime temperature is relatively lower, because the cold air flows. In the case of building, night air flow direction should be considered.
ZONE3 Not suitable for living and newly developing: Newly developing is not recommended, because cold air is producted in this zone.
Degree of recommendation
Land cover improvement
ZONE4
ZONE5
ZONE6
Strongly recommended
Degree of recommendation
Ventilation improvement
Land cover improvement
ZONE7
ZONE8
ZONE9
Strongly recommended
Strongly recommended
Countermeasures menus
Ventilation Improvement (examples)
•Arranging buildings with consideration major wind direction (making ventilation paths)
•Making open space in the direction of land breeze
Land Cover Improvement (examples)
•Greening to surface or building
•Water retentive pavement to road

Fig. 34. Urban Climate Environmental Map at nighttime.

way as in the above section, the correlation coefficient was calculated in ascending order between the average temperature in observations where "DCDS" was more than Y km and "RBB-NNW in two dimensions." Next, the threshold was defined using the relationship between "RBB-NNW in two dimensions" and the average temperature of 27 observations, where Y was 3; the zoning uses that threshold.

For zoning in the mountain area, the area was gradually classified into three zones using the threshold of "ACA": Zone 1, Zone 2, and Zone 3 (Fig. 34).

6.3. Making UECMs

UECMs are made based on the above climate zoning by daytime and at night. Recommendations for planning or usable climatic resources for mitigation are also shown in each zone. In daytime, these are shown based on the results that the influence of sea breeze and ventilation condition in the direction of south-southwest is large in the plains area and the amount of insolation is large in the mountain areas during daytime. Also, at night, these are shown based on the results that the influence of land breeze, surrounding green area and ventilation condition in the direction of NNW is large in the plains area and the amount of cold air is large in the mountain areas. If stakeholders use maps and understand the climatic characteristics of each zone, they can make decision about urban planning, architectural design, and environmental policies based on an urban warming mitigation perspective. For example, these can be used as maps for master plans or to create the guidelines for district planning or urban redevelopment.

7. Conclusion

In this study, previous studies about UECMs were first organized and the three conditions which that should be made in the future were shown. Next, to make such UECMs, a long-term multi-point observation was performed by setting 60 temperature sensors in instrument screens in Hiroshima and the analysis of the relationship between temperature and contributory factors was conducted using the observed data and simulation results. Finally, climate zoning and the construction of UECMs were performed based on the results. The results are as follows:

1) Temperature distribution patterns and their factors in plain and mountain areas differ. Moreover, there are two types of climate characteristics in Hiroshima City due to geographical characteristics from the observation point classification results. Therefore, in Chapter 2, the Hiroshima area is classified into the plains area and the mountain area and these two zones correspond to large climate zoning.
2) With respect to the plains area, multiple regression analysis was performed using the factors DCDS, RBB-SSW, RBB-NNW, NDVI-300, and RA-300, to evaluate the factors comprehensively. As a result, it was found that the influence of DCDS is large, while RBB-SSW also influences the temperature in the daytime. The influence of NDVI-300 is also large, while that of RBB-NNE influences the temperature at night.
3) The mechanism whereby temperature distribution is influenced by DCDS was clarified by using the observed temperature and numerical simulation results. As a result, it was found that the temperature difference between Pattern A and Pattern C is not related to wind

speed distribution but to sensible heat advection. This means that diurnal temperature distribution is affected by sea breeze and the DCDS represents the sea breeze effect.

4) With respect to the mountain area, a multiple regression analysis was performed using the factors AI, TPI, NDVI-300, and ACA, to evaluate the factors comprehensively. As a result, it was found that the influence of TPI is large on the temperature at daytime, except from 9:00 to 12:00. There is also a large influence of ACA on the temperature at night.

In this study, UECMs were constructed in view of the relationship between temperature distribution and its contributory factors. However, it is necessary to further consider the forms of UECMs because they should be easy to use for stakeholders making decisions on urban planning, architectural design, and environmental policy; these are proposed under the assumption that they will be used as a reference. Specifically, it is necessary to perform interview and questionnaire surveys in which stakeholders evaluate the several different types of UECMs, for example, the difference in scale or the numbers of the zone. Based on the results of the surveys, it is recommended that UECMs be systematized in the future.

Acknowledgements

This study was supported by Grant-in Aid for Scientific Research (C) (16K06610) and Grant-in-Aid for Japan Society for the Promotion of Science Fellows (15J06553, 17J07605). The authors thank Environmental Policy Division, Environmental Bureau, the City of Hiroshima and City Planning Division, Urban Development Bureau, the City of Hiroshima. On the field measurement temperature, the authors also thank the elementary school of Hiroshima and Hiroshima Board of Education.

References

Acero, J. A., Arrizabalaga, J., Kupski, S., & Katzschner, L. (2013). Deriving an urban climate map in coastal areas with complex terrain in the Basque Country (Spain). *Urban Climate, 4*, 35–60. https://doi.org/10.1016/j.uclim.2013.02.002.

Alcoforado, M. J., Andrade, H., Lopes, A., & Vasconcelos, J. (2009). Application of climatic guidelines to urban planning. The example of Lisbon (Portugal). *Landscape and Urban Planning, 90*, 56–65. https://doi.org/10.1016/j.landurbplan.2008.10.006.

Amano, N., & Nakagawa, K. (2007). A study on the relationships between temperatures and land-cover characteristics in urban area using LANDSAT TM data. *Bulletin of Toyama Prefectural University, 17*, 108–113. (in Japanese) Retrieved from -, 2019 Retrieved from - http://ci.nii.ac.jp/els/contents110006405433.pdf?id=ART0008405903.

Architectural Institute of Japan (2000). Toshikankyo no klimaatlas kikojoho o ikashita toshizukuri (KlimaAtlas of Urban Environment: Urban planning with using the climate information). *Gyosei* (in Japanese).

Architectural Institute of Japan (2007). Heat island to kenchiku・toshi -taisaku no vision to kadai. (Architecture, city and heat island -vision and challenge of countermeasures-). *Architecture Institute of Japan Series* (in Japanese).

Bureau of the Environment, Tokyo Metropolitan Government (2005). *Guidelines for heat island control measures.* Retrieved fromhttps://www.kankyo.metro.tokyo.jp/en/attachement/heat_island.pdf.

Cai, M., Ren, C., Xu, Y., Dai, W., & Wang, X. M. (2016). Local climate zone study for sustainable megacities development by using improved WUDAPT methodology—A case study in Guangzhou. *Procedia Environmental Sciences, 36*, 82–89. https://doi.org/10.1016/j.proenv.2016.09.017.

Cai, Z., Han, G., & Chen, M. (2018). Do water bodies play an important role in the relationship between urban form and land surface temperature? *Sustainable Cities and Society, 39*, 487–498. https://doi.org/10.1016/j.scs.2018.02.033.

He, X. D., Shen, S. H., Miao, S. G., Dou, J. J., & Zhang, Y. (2015). Quantitative detection of urban climate resources and the establishment of an urban climate map (UCMap) system in Beijing. *Building and Environment, 92*, 668–678. https://doi.org/10.1016/j.buildenv.2015.05.044.

Inter-Ministry Coordination Committee to Mitigate Urban Heat Island (2004). *The policy framework to reduce urban heat island effects.* Retrieved fromhttps://www.env.go.jp/en/air/heat/heatisland.pdf.

Irie, T., & Hirano, K. (2001). Effect of open space in its surrounding area and effective form of open space on air temperature: A case study on Tokyo and Saitama area. *City Planning Review. Special Issue, Papers on city planning, 36*, 277–282. https://doi.org/10.11361/journalcpij.36.277 (in Japanese).

Ishida, K., Munehiro, K., Matsusita, T., & Horikoshi, T. (2013). Field observation on influence of mountains and rivers on urban air temperature distribution in Gujo-Hachiman as intermediate and mountainous area. *Japanese Journal of Biometeorology, 50*(1), 37–47. https://doi.org/10.11227/seikisho.50.37 (in Japanese).

Itada, M. (2006). Promotion of heat island measures in Osaka Prefecture. *Environmental Conservation Engineering, 35*(7), 474–478. https://doi.org/10.5956/jriet.35.474 (in Japanese).

Junimura, Y., & Watanabe, H. (2008). Study on the effects of sea breeze for decreasing urban air temperatures in summer: Analyses based on long-term multi-point measurements and observed wind conditions. *Journal of Environmental Engineering AIJ, 73*(623), 93–99. https://doi.org/10.3130/aije.73.93 (in Japanese).

Kitao, N., Moriyama, M., Takebayashi, H., & Tanaka, T. (2012). A Study on making method of climate atlas in Osaka region. *AIJ Journal of Technology and Design, 18*(38), 255–258. https://doi.org/10.3130/aijt.18.255 (in Japanese).

Kiyota, T., Taniguchi, A., Kiyota, N., & Nakamura, Y. (2007). The study on countermeasures against the heat island phenomenon in the urban area: Part 2 the multiple regression analysis to the relationship between city temperature and the land cover in summer. *Journal of Environmental Engineering AIJ, 72*(64), 57–63. https://doi.org/10.3130/aije.72.57_2 (in Japanese).

Kusaka, H., Kondo, H., Kikegawa, Y., & Kimura, F. (2001). A simple single-layer urban canopy model for atmospheric models: Comparison with multi-layer and slab models. *Boundary-layer Meteorology, 101*(3), 329–358. https://doi.org/10.1023/A:1019207923078.

Miyata, K. (1982). The sea and land breeze in Hiroshima Prefecture. *Keisuisya* (in Japanese).

Mori, H., Kitada, T., & Iyoda, K. (1998). Vertical structures of land and sea breezes in the Nohbi plain during a passage of an anticyclone over the central Japan. *Tenki, 45*(7), 515–530. (in Japanese) Retrieved from -, 2019 Retrieved from http://www.metsoc.jp/tenki/pdf/1998/1998_07_0515.pdf.

Moriyama, M., & Takebayashi, H. (1998). *Study on klimaatlas for urban environment: Example of Kobe area. Summaries of Technical Papers of Annual Meeting, D-*1911–912 (in Japanese).

Moriyama, M., & Takebayashi, H. (1999). Study on making method of “klimatope” map based on normalized vegetation index and one dimensional heat budget model. *Journal of Architecture and Planning AIJ, 64*(518), 61–65. https://doi.org/10.3130/aija.64.61_2 (in Japanese).

Mouri, K., Oba, H., Mochida, A., Yoshino, H., & Watanabe, H. (2008). Zoning of the urban climate in Sendai for selecting the appropriate countermeasures against urban heat island effects (Part3) Zoning method to include the influence of air exchange rate of outdoor space and latent heat balance. *Proceedings of National Symposium of Wind Engineering, 20*, 97–102. (in Japanese) Retrieved from -, 2019 Retrieved from https://www.jstage.jst.go.jp/article/kazekosymp/20/0/20_0_17/_pdf/-char/ja.

Nabeshima, M., Nishioka, M., & Nakao, M. (2008). Horizontal temperature variation in the Osaka Plain in summer. *Transactions of the Society of Heating, Air-conditioning and Sanitary Engineers of Japan, 140*, 1–10. https://doi.org/10.18948/shase.33.140_1 (in Japanese).

Narumi, D., Habara, K., & Mizuno, M. (2009). Development of an environmental thermal load evaluation system for the purpose of mitigating urban thermal environment: part2 framework of the weighted heat flux evaluation method and example of evaluation at building level. *Transactions of the Society of Heating, Air-conditioning and Sanitary Engineers of Japan, 147*, 17–28. https://doi.org/10.18948/shase.34.147_17 (in Japanese).

Narumi, D., Mizuno, M., & Shimoda, Y. (2002). Fundamental investigation on guidelines for regional and architectural planning with climatic characteristics taken into account: Through climatic analyses on hillside area around cities. *Journal of Architecture and Planning AIJ, 67*(561), 93–100. https://doi.org/10.3130/aija.67.93_5 (in Japanese).

Ng, E., & Ren, C. (2015). *THE URBAN CLIMATIC MAP: A methodology for sustainable urban planning.* Routledge.

Noguchi, S., Tanaka, T., & Sadohara, S. (2014). Analysis on the factors of summer temperature in the basin city: Measurement results and analysis by GIS. *AIJ Journal of Technology and Design, 20*(46), 1029–1034. https://doi.org/10.3130/aijt.20.1029 (in Japanese).

Ogawa, T., Murakawa, S., Nishina, D., Tanaka, T., Fukagawa, K., & Takahashi, I. (2011). A study on the effect of land use and insolation environment on surrounding air temperature in mountain area: Measurement results and analysis by GIS. *AIJ Journal of Technology and Design, 17*(35), 245–248. https://doi.org/10.3130/aijt.17.245 (in Japanese).

Ojima, T. (2010). Midori mizu kaze o ikashita kenchiku・toshikeikaku. (THE COOL CITY strategy of heat island mitigation: Architecture and Urban planning utilizing green, water and wind). *Building Technology*.

Osaka prefecture and Osaka city (2015). *Osaka heat island taisaku suishin keikaku. (Osaka heat island measure promotion plan)* (in Japanese)http://www.pref.osaka.lg.jp/attach/1144/00182871/osakaheatkeikaku.pdf.

Ren, C., Lau, K. L., Yiu, K. P., & Ng, E. (2013). The application of urban climatic mapping to the urban planning of high-density cities: The case of Kaohsiung. *Taiwan. Cities, 31*, 1–16. https://doi.org/10.1016/j.cities.2012.12.005.

Ren, C., Spit, T., Lenzholzer, S., Yim, H. L. S., Heusinkveld, B., van Hove, B., et al. (2012). Urban climate map system for Dutch spatial planning. *International Journal of Applied Earth Observation and Geoinformation, 18*, 207–221. https://doi.org/10.1016/j.jag.2012.01.026.

Sakai city (2008). *Sakai heat island taisaku suishin keikaku (Sakai heat island measure promotion plan)* (in Japanese) Retrieved December 10, 2017 fromhttp://www.city.sakai.lg.jp/shisei/gyosei/shishin/kankyo/ondanka/heat_island.html.

Samata, M., Inoue, T., Fukuda, A., & Hirasawa, S. (2006). On the method making out heat environmental mapping at Yokohama city. *Annual Report of Yokohama Environmental Research Institute, 30*, 56–59. (in Japanese) Retrieved from -, 2019 Retrieved from http://www.city.yokohama.lg.jp/kankyo/mamoru/kenkyu/shiryo/pub/pub0154/

pdf/pub015411.pdf.
Skamarock, W. C., Klemp, J. B., Dudhia, J., Gill, D. O., Barker, D. M., Duda, M. G., et al. (2008). *A description of advanced research WRF version3. NCAR/TN-475+STR*.
Stewart, I. D., & Oke, T. R. (2012). Local climate zones for urban temperature studies. *Bulletin of the American Meteorological Society, 93*(12), 1879–1900. https://doi.org/10.1175/BAMS-D-11-00019.1.
Takane, Y., Ohashi, Y., Kusaka, H., Shigeta, Y., & Kikegawa, Y. (2013). Effects of synoptic-scale wind under the typical summer pressure pattern on the mesoscale high-temperature events in the Osaka and Kyoto urban areas by the WRF model. *Journal of Applied Meteorology and Climatology, 52*, 1764–1778. https://doi.org/10.1175/JAMC-D-12-0116.1 (in Japanese).
Takebayashi, H., & Moriyama, M. (2002). Filling process in a valley and outflow process into a built-up area of cold air drainage on summer night. *Journal of Environmental Engineering AIJ, 67*(558), 57–61. https://doi.org/10.3130/aija.67.57_2 (in Japanese).
Takebayashi, H., Akagawa, H., & Moriyama, M. (2010). Possibility study on cold air drainage from a large roof garden. *Summaries of Technical Papers of Annual Meeting, D-1*, 981–982 (in Japanese).
Takeuchi, S. (1987). Estimation of vegetation cover rate within one pixel using the vegetation index of satellite images. *Journal of the Japan Society of Photogrammetry and Remote Sensing, 26*(4), 4–12. https://doi.org/10.4287/jsprs.26.4_4 (in Japanese).
Tanaka, T., & Moriyama, M. (2004). *Application of GIS to make 'urban environmental climate map' for urban planning. Fifth Conference on Urban Environment*. Retrieved December 10, 2017 from https://ams.confex.com/ams/AFAPURBBIO/techprogram/paper_79052.htm.
Tanaka, T., & Moriyama, M. (2011). Urban environmental climate maps for supporting environmental and urban planning works in local government: case study in city of Sakai, Osaka. *AIJ Journal of Technology and Design, 17*(36), 687–692. https://doi.org/10.3130/aijt.17.687 (in Japanese).
Tanaka, T., Mikasa, T., Uchihira, T., Yamazaki, Y., & Shigemura, T. (2014). A study on application of GIS for mapping "YATO" unit: In case of Yokohama. *Journal of Architecture and Planning AIJ, 79*(698), 933–938. https://doi.org/10.3130/aija.79.933 (in Japanese).
Tanaka, T., Yamashita, T., & Moriyama, M. (2007). Community planning workshop by using "urban environmental climate map": Practice of workshop in the Komagabayashi neighborhood, Nagata, Kobe. *Journal of Environmental Engineering AIJ, 72*(611), 91–98. https://doi.org/10.3130/aije.72.91_1 (in Japanese).
Terano, T. (2012). How to convince social simulation technologies. *Japan Science Support Foundation, 17*(2), 45–47. https://doi.org/10.5363/tits.17.2_45 (in Japanese).
The Ministry of Land, Infrastructure, Transport and Tourism (2015). *Kokudo kotsusho kikohendo tekio keikaku (Practical guidelines on strategic climate change adaptation planning)* (in Japanese) Retrieved from Retrieved from -http://www.mlit.go.jp/common/001111532.pdf.
Verein Deutscher Ingenieure (1997). *Environmental meteorology climate and air pollution maps for cities and regions.* 3787, Part1.
Verein Deutscher Ingenieure (2015). *Environmental meteorology climate and air pollution maps for cities and regions.* 3787, Part1.
Vitanova, L. L., & Kusaka, H. (2018). Study on the urban heat island in Sofia City: Numerical simulations with potential natural vegetation and present land use data. *Sustainable Cities and Society, 40*, 110–125. https://doi.org/10.1016/j.scs.2018.03.012.
Watanabe, H., & Junimura, Y. (2004). Kaze to nihon no machizukuri –sendai no kaze (Kuki to mizu no seitai dezain) (Wind and urban planning in Japan -the wind in Sendai (The ecological for air and water)). *Bio City,* 27.